


RESEARCH

Open Access



Analysis of mosaic mortars from the Roman, Byzantine and Early Islamic periods sourced from Gerasa's Northwest Quarter

Richard J. Ball^{1*} , Martin P. Ansell¹ , Tuğçe Büşra Su-Cadirci² , Vahiddin Alperen Baki¹ , Philip J. Fletcher³ , Achim Lichtenberger⁴ , Rubina Raja⁵  and Will Wootton⁶ 

Abstract

This study analyses and compares around 650 years of mosaic mortar production spanning the Roman, late Roman and Umayyad periods, at Gerasa/Jerash in Jordan, offering a better understanding of composition, structural features, and manufacturing processes. It assesses the value of optical and electron microscopy examination of morphological and textural features, pore structure using MIP, and composition studies using EDX, XRD, FTIR, TGA, and Raman spectroscopy. The study indicated high density lime adhesive was used compared to other mortars. Wood was used as a fuel when producing the lime and natural fibres were incorporated when manufacturing mortars. Aggregates were primarily calcitic with a small proportion of silica-based aggregates. Key outcomes of the study conclude that early Roman mortars were of highest quality, which was demonstrated through the careful selection of materials including different stone for lime and tesserae, and differences between layers. Late Roman mortars used the same slaked lime plus fibres and charcoal. Mortars dating from the Umayyad period also had the same higher lime content than late Roman, but higher porosity with fibres and charcoal. In general, the mortars showed slight differences in content and aggregate; different stone for lime and tesserae. The research attests to underlying traditions as well as changes in mortar mixes and methods according to context and time. The resulting data is contextualized within local and regional approaches.

Keywords Lime, Mosaic, Gerasa

Introduction

The excavations of the Danish-German Jerash Northwest Quarter Project have produced mortars used in a variety of contexts over the occupation of the site. Whereas previous analyses have focused on mortar from functional contexts, in particular the cisterns [1, 2], this scientific investigation takes the mosaics mortars, which belong to decorative ensembles, as its starting point. A major achievement of this study is the characterization of mortars to provide new knowledge about the production of lime at Jerash, the mortar mix designs used for the mosaic floors and their manufacturing methods. Mosaics are multi-material media and the foundations form a critical component in ensuring their basic functionality. Where possible, separate

*Correspondence:

Richard J. Ball
r.j.ball@bath.ac.uk

¹ Centre for Integrated Materials, Processes & Structures (IMPS),
Department of Architecture and Civil Engineering, University of Bath,
Bath BA2 7AY, UK

² Department of Architecture, Abdullah Gul University, 38080 Kayseri,
Turkey

³ Imaging Facility, University of Bath, Bath BA2 7AY, UK

⁴ Institut Für Klassische Archäologie Und Christliche Archäologie/
Archäologisches Museum, Universität Münster, Domplatz 20-22,
48143 Münster, Germany

⁵ Department of Classical Studies, The Danish National Research
Foundation's Centre of Excellence for Urban Network Evolutions (UrbNet),
Moesgård Allé 20, 4230-230, DK-8270 Højbjerg, Denmark

⁶ Classics Department, King's College London, The Strand, London WC2R
2LS, UK



© The Author(s) 2024. **Open Access** This article is licensed under a Creative Commons Attribution 4.0 International License, which permits use, sharing, adaptation, distribution and reproduction in any medium or format, as long as you give appropriate credit to the original author(s) and the source, provide a link to the Creative Commons licence, and indicate if changes were made. The images or other third party material in this article are included in the article's Creative Commons licence, unless indicated otherwise in a credit line to the material. If material is not included in the article's Creative Commons licence and your intended use is not permitted by statutory regulation or exceeds the permitted use, you will need to obtain permission directly from the copyright holder. To view a copy of this licence, visit <http://creativecommons.org/licenses/by/4.0/>. The Creative Commons Public Domain Dedication waiver (<http://creativecommons.org/publicdomain/zero/1.0/>) applies to the data made available in this article, unless otherwise stated in a credit line to the data.

layers of the bedding were examined to assess the complete sequence of the foundations and the relationships between the mortar mixes across the production stages, each with their own specific purpose within the overall mosaic. The intention is to understand how and why the mortars were used at different points in the process, and more broadly at various times and places during the life of the Northwest Quarter of the site as well as to provide a basis for future discussions of mortars in the region from a comparative perspective.

The Danish-German Jerash Northwest Quarter Project began in 2011 and ended with a study campaign in 2017. The project has examined an area of about 4 hectares located on the highest point of the walled city in what can be termed a peripheral area sitting above the Roman period Artemision in the western part of the city [3, 4]. The Decapolis city of Gerasa flourished in the Roman, Byzantine and early Islamic periods until an earthquake brought a halt to most urban activity at the site in 749 AD [5]. While we know that the site existed before the Roman period, the archaeology tells us very little about the earlier phases [6]. Most archaeological finds come from the early Roman imperial period onwards. After the earthquake the Northwest Quarter was abandoned and only resettled again in the Middle Islamic period [7–9].

The archaeological work undertaken within the framework of the Danish-German Jerash Northwest Quarter Project has brought to light complexes from the Roman and later periods, and material from several of these contexts has been included in this study. Mosaics have been one of the main interests of research at Jerash since the first excavations in the early twentieth century [10–13]. The artistic medium tends to survive well; tesserae and fragments from floors and walls have been found scattered across the site. Jerash is most well-known for its Byzantine mosaics which embellished religious buildings starting in the fifth century AD, with production increasing rapidly during the sixth and then declining in the early seventh century [14–18].

Although the Northwest Quarter project has contributed to our understanding of Byzantine religious mosaics with the discovery of the so-called Mosaic Hall [19, 20], this paper focuses on the less well known, and much rarer, mosaics from the Roman and Islamic periods. There are a handful of Roman mosaics from Jerash and those from the early Umayyad period are the only surviving examples [14, 21–23]. These materials, therefore, offer significant new insights into the decoration and associated production technologies at these times. Byzantine mosaic fragments are included to provide context so that the complete chronological sequence is considered and understood.

The foundations of a tessellated mosaic are made up of a series of superimposed layers, each consisting of lime mortar mixed with aggregates at different ratios. The number of layers varies according to the context but is generally between two, at a minimum, and four as specified by Vitruvius (*De Architectura* 7.1). The lower layers are coarser being made up of larger stones and other aggregates such as broken ceramic or recycled building materials, sometimes even shells [24]. They become progressively finer and smaller towards the setting bed, which is usually a purer lime mixed with powdered stone, including volcanic rocks, or terracotta, into which the tesserae were embedded. The mosaic's surface is normally grouted using another mix of lime mortar with microscopic additives, resulting in the grout filling the interstices between the tesserae. Different terminologies are used for these layers, some following Vitruvius. In this study, a simplified, contemporary vocabulary has been applied with 'base' being used for layers preceding the setting bed and 'adhesive' for the setting bed itself.

Lime mortars and plasters can be classified as either hydraulic or non-hydraulic depending on the composition [25, 26]. They are traditionally manufactured by burning [27, 28] a source of calcium carbonate to form calcium oxide, which can then be hydrated to form calcium hydroxide [29, 30]. Historic mortars are often less homogeneous and contain phases such as unburnt lime, pure lime lumps, carbon [31] and organic materials [32] which are commonly identifiable.

The samples investigated attest to around 650 years of mosaic mortar production at Gerasa in Jordan. This study has employed complementary techniques including, scanning electron microscopy, energy dispersive X-ray spectroscopy, X-ray diffraction [33, 34], Raman spectroscopy, Fourier transform infrared spectroscopy, thermogravimetric analysis, mercury intrusion porosimetry and acid dissolution, to better understand the composition, structural features and manufacturing processes of the mosaics from the Northwest Quarter.

Experimental methods

The following section details the experimental methods applied during this study.

Sampling methodology

Samples were selected from archaeological contexts belonging to trenches excavated by the Northwest Quarter Project (Fig. 1). It is noteworthy that it was not possible to differentiate between grout and adhesive for the specimens in this study.

Seven mosaic fragments with their mortar bedding intact were chosen for sampling (Fig. 2; Table 1). Fragments were selected based on size, preservation,

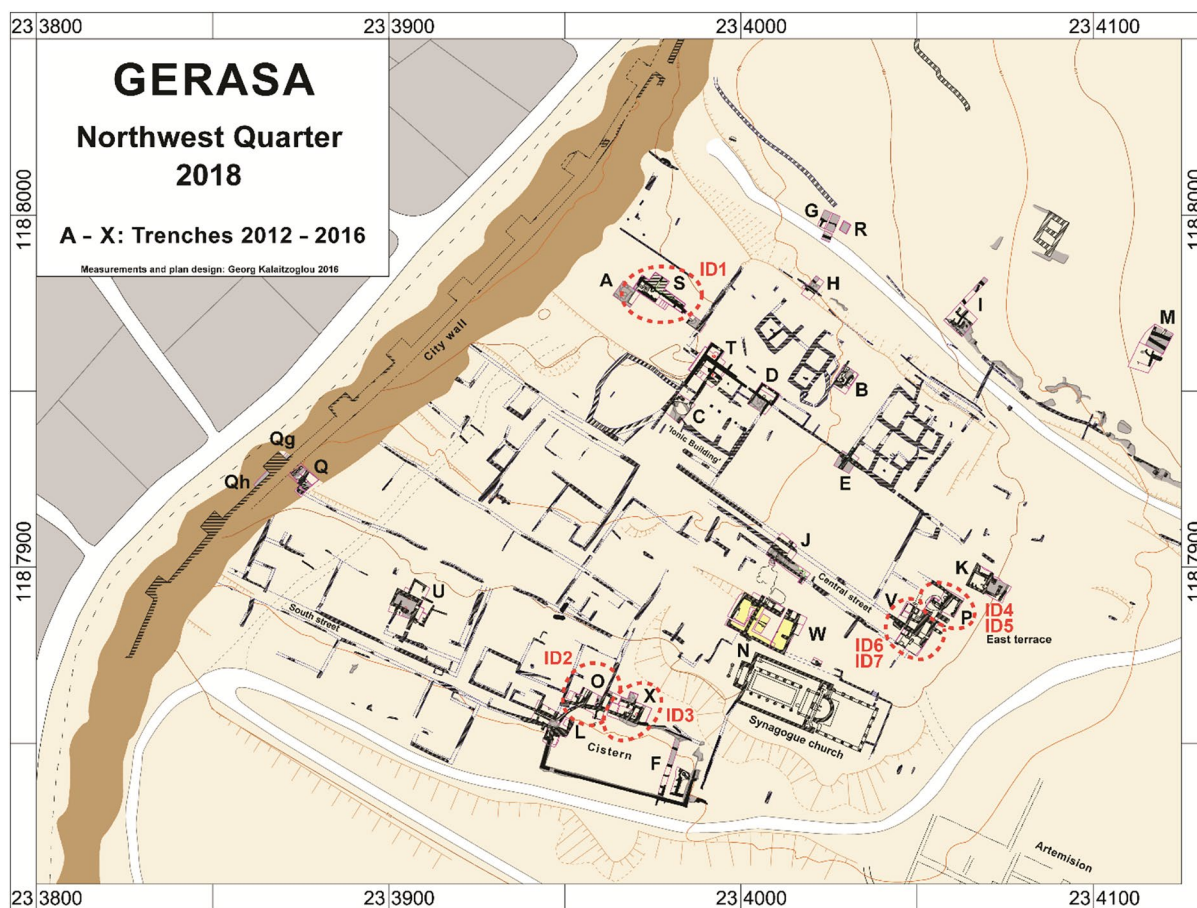


Fig. 1 Locations of samples ID1–ID7 selected from archaeological contexts belonging to trenches excavated by the Northwest Quarter Project

chronology, and location. They are all duplicate examples known in series from the same trenches so that destructive investigations could be adopted if deemed necessary. The samples come from five trenches that produced fragmentary pieces of mosaic, in secondary contexts, dating from the early Roman through to the early Umayyad periods. The chronological range of the different flooring mortars offers the opportunity to assess similarities and differences between the mortar mixes according to the specificity of their context, function and date.

The earliest sample (ID1) was excavated in trench S. The fragment comes from a Roman-period floor which probably belonged to a high-status monumental building constructed in the late first or early second century AD [35, 36]. With other pieces from the same pavement, it was intentionally deposited in a cistern alongside parts of the structure's fabric in the Late Roman period (third to fourth centuries AD). Two samples, one from trench O (ID2) and the other from trench X (ID3), were found on a terrace that was transformed during the Byzantine and Umayyad periods [1, 35, 37]. These fragments both likely

came from the same pavement of Late Roman or early Byzantine date, which was broken up at some time before the Byzantine remodelling of the area. Four samples were chosen from trenches P and V (ID4, ID5, ID6, and ID7). These were excavated amongst the collapse of upper storey floors from an Umayyad house, the so-called House of the Tesserae, destroyed during the earthquake of 749 CE [35–38].

The samples cover the major mosaic finds, except for the in-situ tessellated pavements from the so-called Mosaic Hall [19, 20, 37–39], and allow investigation of the associated manufacturing processes at each stage of their production. Together with the analytical techniques, the research was designed to characterize the composition, structural features and elucidate information regarding their production.

Analysis and characterisation of specimens

The specimens were analysed and characterized using the following methods.

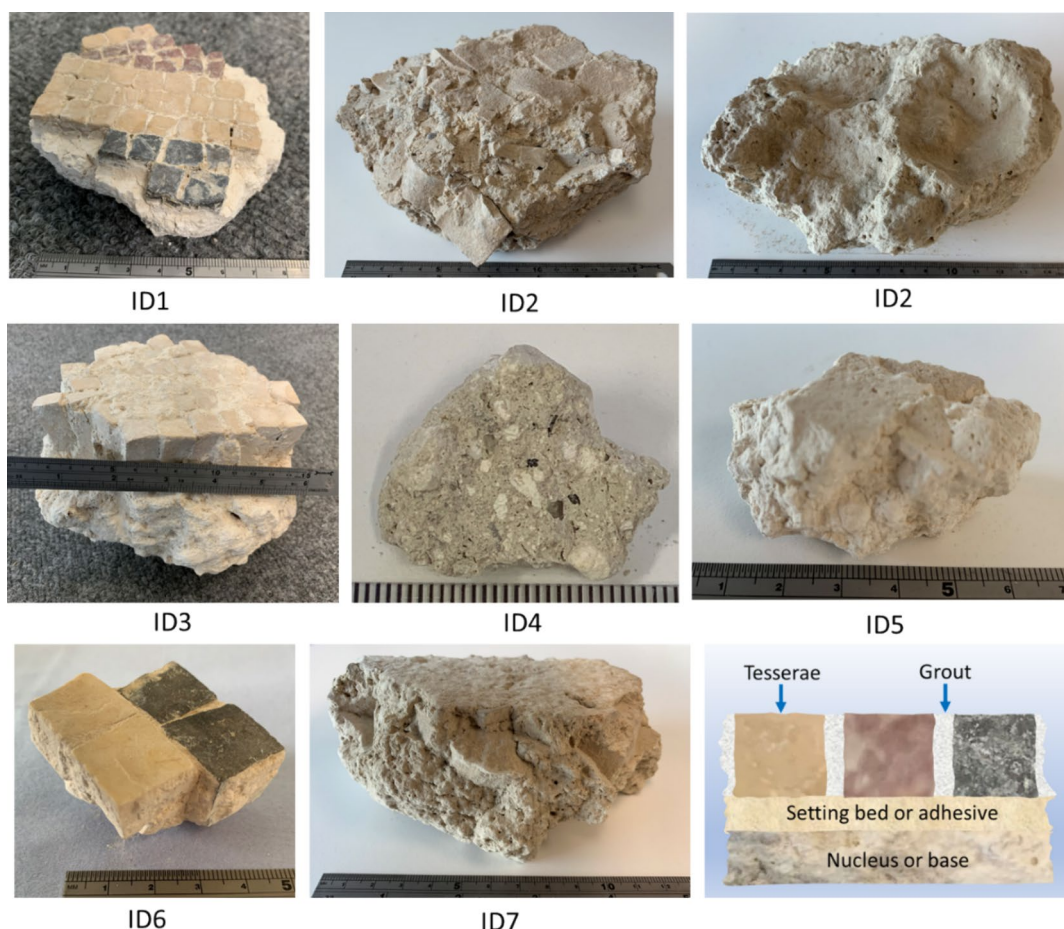


Fig. 2 Photographs of the mosaic fragments collected. ID1: specimen of Roman date from trench S; ID2 (right hand side image shows underside of sample) and ID3: specimens of Late Roman and Byzantine date from trenches of O and X; ID4-ID7 Specimens of Early Islamic date from trenches P and V; (i) Cross sectional diagram of mosaic structure showing tesserae, grout, adhesive and mortar

Determination of binder/aggregate ratio

The historic mortars and grouts acid dissolution test was performed using a 3/7 solution of hydrochloric acid and distilled water at room temperature. The HCl solution (30 mL, 36 wt.%) was gradually added to the sample-dispersed deionised water solution (70 mL). During dissolution, the pH was periodically monitored, and additional acid was added if necessary. Total dissolution was assumed when the pH level remained constant. The insoluble fractions were vacuum filtered and rinsed with deionised water, and the residue was dried and weighed. Gravimetry was used to determine the aggregate ratio of the historical samples.

Optical and electron microscopy, and EDX analysis

Optical microscopy was carried out using a Keyence VHX-6000 Series 3D Imaging Microscope. A Z20 lens was used to view a fracture surface at magnifications of $\times 30$, $\times 50$, $\times 100$, $\times 150$, $\times 200$. The microscope was

operated in normal imaging mode for focused images of a particular region of a sample and image stitching was employed to enable imaging of the full sample in one picture. White balance enabled more effective distinguishing of coloured regions. Polished thin sections were prepared by Hands On Thin Sections Ltd from samples impregnated under vacuum with a low viscosity epoxy resin. The samples were analysed with a Leica DM750 P microscope using both cross polarised and transmitted light as well as incident light. Three representative images were selected from each specimen for analysis of aggregate and pore sizes. The total area of each image was equal to 10.89×6.08 mm, therefore all three images had a total area of 66 mm^2 . Following calibration, the size of each pore and aggregate located within the image was measured using image J Version 1.53 k. Pore and aggregate dimensions were categorised between 0.015 and 1 mm and plotted as a frequency histogram.

High magnification images of the samples were produced using either a JEOL JSM-6480LV variable pressure scanning electron microscope (SEM) equipped with an Oxford Instruments INCA X-act energy dispersive X-ray analyser (EDX) or a Hitachi SU3900 large chamber, variable pressure SEM with an Oxford Instruments Ultim Max 170 mm² (EDX) analyser. Both these systems allowed mapping, line scan, point ID and quantitative analysis functions which were used where appropriate. Images were obtained at magnifications from 50× to 5000×. Additional images of polished cross sections of the red, black and white tesserae were obtained at magnifications of 3000×. Elemental analysis scans using EDX were performed at 10 kV and all elements analysed were normalised. Surface scans were performed over representative rectangular areas which were relatively flat and had edges ranging from approximately 50–1000 μm. Between 2 and 4 such areas were analysed and the average elemental composition is reported.

Mercury intrusion porosimetry (MIP)

The percentage porosity by volume and pore size distribution of the mortars was determined using Pascal 140 and Pascal 440 mercury intrusion porosimeters, combining low- and high-pressure analysis up to 400 MPa utilising a glass dilatometer. Testing was conducted in two phases, the first at low pressure from 0 to 100 kPa and the second at high pressure up to 400 MPa.

Thermogravimetric analysis (TGA)/Differential scanning calorimetry (DSC)

The thermogravimetric measurements of the historic mortars and grouts were conducted using the Netzsch Sta 449F1 Jupiter machine. The heating program ramped from 50 to 950 °C at a constant heating rate of 10 °C/min under inert N₂ with a 50 mL/min gas flow.

X-ray diffraction (XRD)

The crystal structures of the historic mortars and grouts were determined using a STOE STADI P X-ray diffractometer employing Cu-K_α radiation with a wavelength of 1.5408 Å. The tests were conducted with a step size of 0.015° from 5° to 60° (2θ). Samples of the mortars were prepared by breaking small representative pieces of the mortar and adhesive, where applicable. They were then crushed to a fine powder. XRD analysis was also carried out on the residue remaining following acid dissolution.

Fourier transform infrared spectroscopy (FTIR)

The FTIR results were obtained using the attenuated total reflection (ATR) method using a Perkin Elmer Frontier Instrument. The FTIR spectra were recorded between

wavenumber 600 and 4000 cm⁻¹, with 10 repeated scans at the resolution of 4 cm⁻¹.

Raman spectroscopy

Raman spectroscopy was carried out using a Renishaw inVia system and WiRe 4.0 software for peak fitting and deconvolution of the spectra. The system was equipped with red and green diode lasers with wavelengths and powers of 785 nm/140 mW and 532 nm/69 mW respectively. The analyses were performed by focusing the laser with objective magnification×50 onto the sample surface through a Leica optical microscope, corresponding to a laser spot diameter of approximately 2 μm. The laser power at the specimen surface was of the order of 3mW and an acquisition time of 10 s was used for each spectrum over the wavenumber range 100–2000 cm⁻¹.

Results

Optical and electron microscopy

Optical microscopy was carried out on fracture surfaces to reveal sub mm features and polished thin sections were imaged to determine porosity and aggregate shapes, sizes and mineralogy. Scanning electron microscopy was applied to fracture surfaces to obtain images at high magnification and reveal the finer microstructural features. Figures 3, 4 and 5 present a selection of images that represent the key features identified in the Roman mortars from the Northwest Quarter (ID1), Late Roman and Byzantine mortars (ID2 and ID3), and the upper floors of the Umayyad building referred to as the 'House of the Tesserae' (ID4–ID7). Previous electron microscopy studies at Jerash, carried out by Hamarneh and Abu-Jaber, reported on the microstructures of representative mortars from the Church of John the Baptist which was built in 531 AD. Several different features observed including fine and re-crystallised grains, overgrowth, plated calcite crystals, and euhedral calcite crystals can be compared to the mortars analysed from the Northwest Quarter noting that those from trench X are probably closest in date [40].

All images in Fig. 3a–d relate to ID1. Figure 3a shows a beige underlying mortar coated in white fine calcite crystals of higher purity. Figure 3b displays basalt (3b.1), a fine-grained, igneous rock composed mainly of plagioclase and pyroxene which looks very similar to amphibole (3b.2) also identified by Rispoli [41], and a black and white speckled crystalline aggregate particle (3b.3) of microscopic silica with dolomite and calcite [42]. Figure 3c is an SEM image of a fracture surface distinguished by areas of calcite crystals and a region of finer ones (3c.4). Figure 3d shows an adhesive layer that has a denser structure and contains hollow fibres coated in well-formed euhedral calcite crystals (3d.5–6), many of which are sub-micron in size but are still

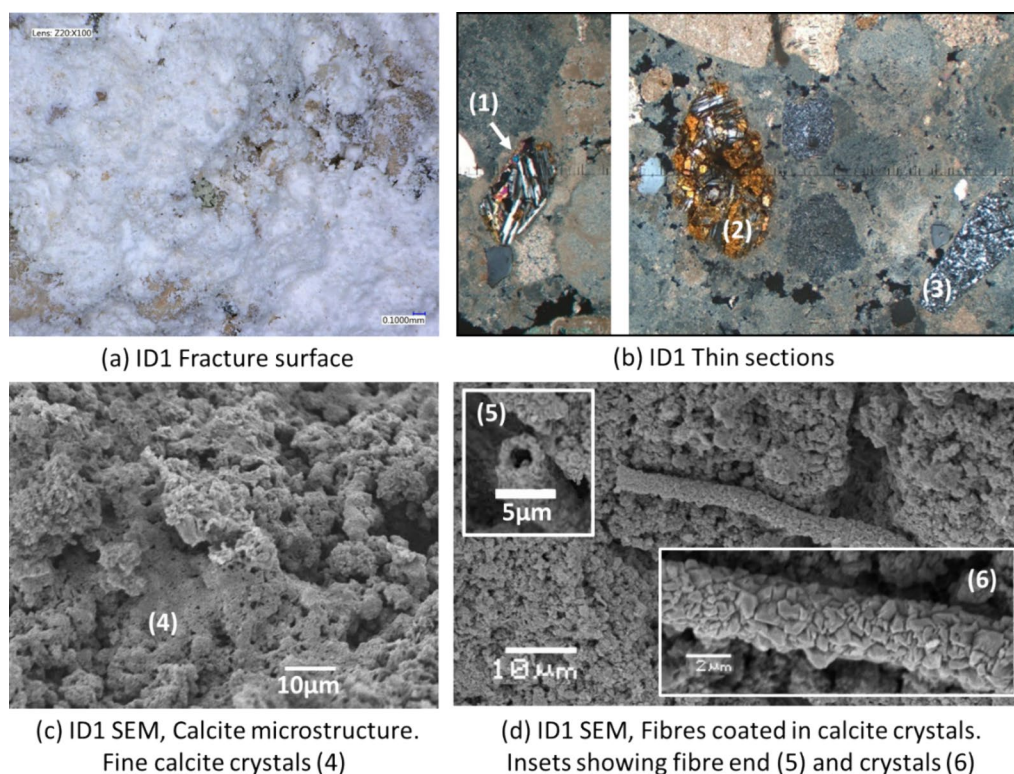


Fig. 3 Roman mortar from the Northwest Quarter (ID1b): **a** Optical microscopy of fracture surface showing white surface crystals covering a brown sublayer; **b** Transmission polarised image of thin sections showing basalt (1), amphibole (2), microscopic silica with dolomite and calcite (3); **c** SEM image of fracture surface showing areas of calcite crystals and a region of fine calcite crystals (4); **d** Fracture surface showing organic fibres coated with angular calcite crystals, top inset (5) shows a cross section of fibre and hollow structure, bottom inset (6) shows higher magnification of surface crystals. (1 unit on thin section images = 0.0267 mm)

easily discernible in the SEM images. The morphology of these crystals is apparent in Fig. 3d. The prevalence of fine-grained crystals is consistent with the work of Harmarneh which reports finer-grained textures in mosaic floors [40]. The absence of any hydraulic phases such as silicates or aluminosilicates is also noteworthy as this supports the observation that these mortars are non-hydraulic and is also in agreement with existing studies [43, 44]. In summary, the mortar adhesive described here has a distinctly Roman character, distinguished by its lack of hydraulicity, the predominance of fine-grained calcite crystals, a thick adhesive layer, and an empirical approach to materials science, as demonstrated by SEM imaging and corroborating academic sources.

Figure 4a (ID2) shows a light grey coloured lime mortar with a granular texture and some charcoal fragments approximately 1 mm across visible underneath the surface (4a.1) and smaller sub-millimeter fragments distributed over the surface. Figure 4b is a SEM image of a typical charcoal particle. The polarised thin section image in Fig. 4c shows numerous aggregate particles of different mineralogy and a charcoal fragment. Figures 4d–e

present some aggregate particles with coloured mineral phases which resemble pyroxenes [45]. Figure 4g (ID3) shows a similar beige coloured mortar to that observed for ID1 (Fig. 3a), however, the white layer of calcite crystals is much sparser. Organic fibres are clearly visible in the optical image (Fig. 4g.1). These look similar to straw fibres identified by Stefanidou [46] in 13th-century Byzantine renders [47]. The fracture surface contains several rounded indents which may have formed from aggregated particles detaching from the surface when preparing the sample. The thin section (Fig. 4h), shows a very uniform structure with no aggregates visible. The SEM images in Fig. 4i–k highlight the porous structure and the presence of wood and fibrous materials. Figure 4k shows some scalenohedral calcite crystals. The corresponding EDX spectrum shown in Fig. 4l confirms the expected composition for calcite of calcium, carbon, and oxygen. Trace amounts of aluminium, silicon and magnesium are also present. In summary, the mortar samples ID2 and ID3 display characteristics commonly associated with Late Roman and Byzantine periods. Specifically, ID2 showcases a light grey lime mortar with granular

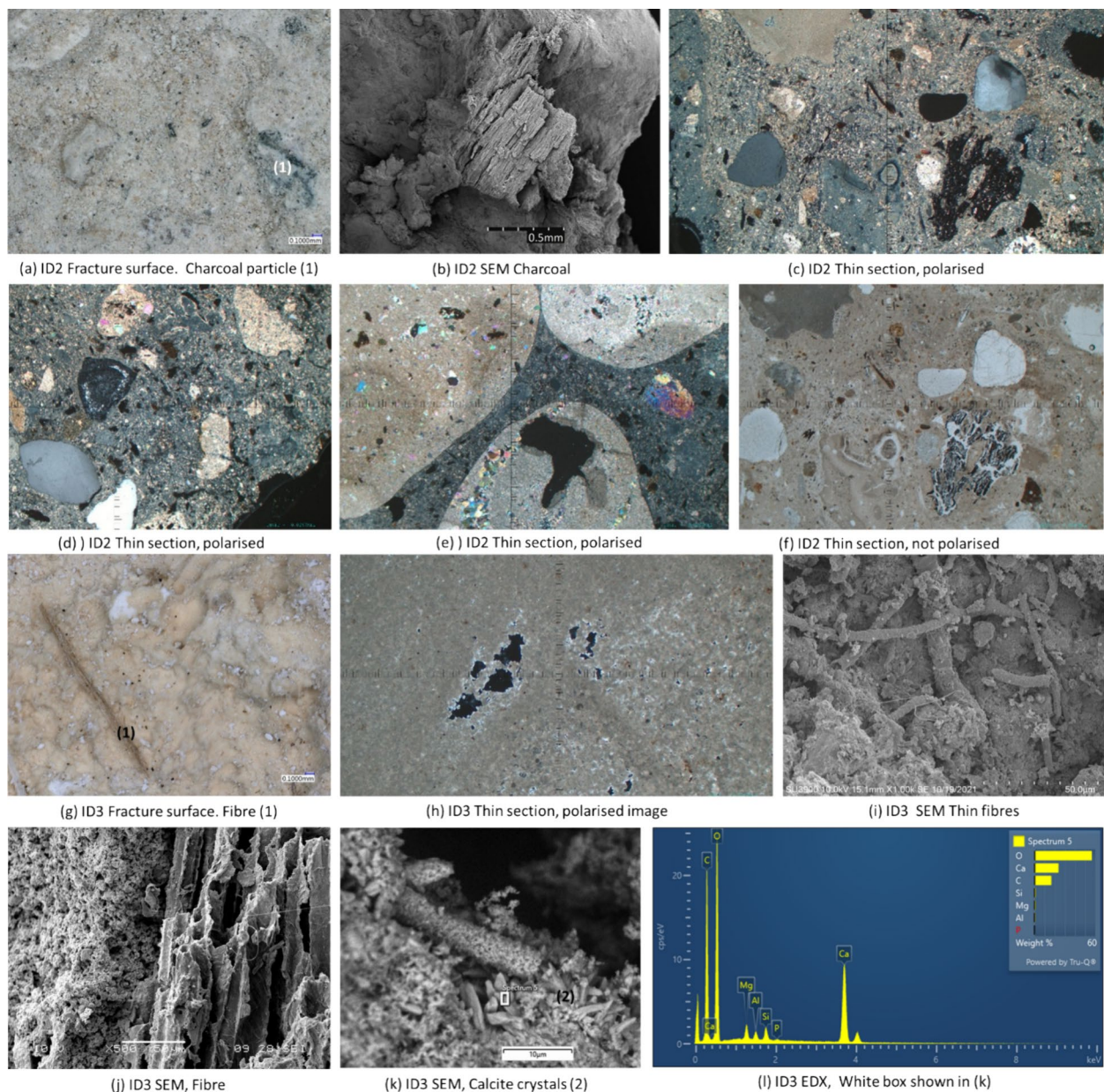


Fig. 4 Microscopy images and EDX analysis of Late Roman and Byzantine mortars ID2 and ID3b: **a** Optical microscopy image of ID2 fracture surface showing grey granular texture with black charcoal particles (1); **b** SEM image of charcoal fragment revealing cellular structure of wood; **c** ID2 Transmission polarised image showing aggregates and charcoal particle; **d** ID2 thin section polarised image showing olivine particles; **e** ID2 thin section polarised image showing olivine particles within lime nodule; **f** ID2 transmission image showing range of different sized mineral aggregates and charcoal particle revealing the internal voids as white; **g** ID3 optical image showing brown mortar with some white calcite crystals and a plant fibre (1); **h** ID3 thin section polarised image revealing a fine homogeneous structure with some porosity and no aggregate particles; **i** SEM image of organic fibres within mortar coated with calcite; **j** SEM image of organic fibre cellular structure visible in adhesive phase; **k** SEM image of organic fibre and scalenohedral calcite crystals (2); **l** EDX spectrum of area indicated by white rectangular box in (k). (1 unit on thin section images = 0.0267 mm)

texture and charcoal fragments. These are features seen in both periods but are particularly reminiscent of Late Roman mortar compositions. This is further evidenced by the varied mineralogy of aggregate particles and the

presence of charcoal, often used in Roman constructions for enhanced structural properties. In contrast, ID3 displays features that are more closely aligned with Byzantine mortars. It has a beige coloration, similar to ID1, but

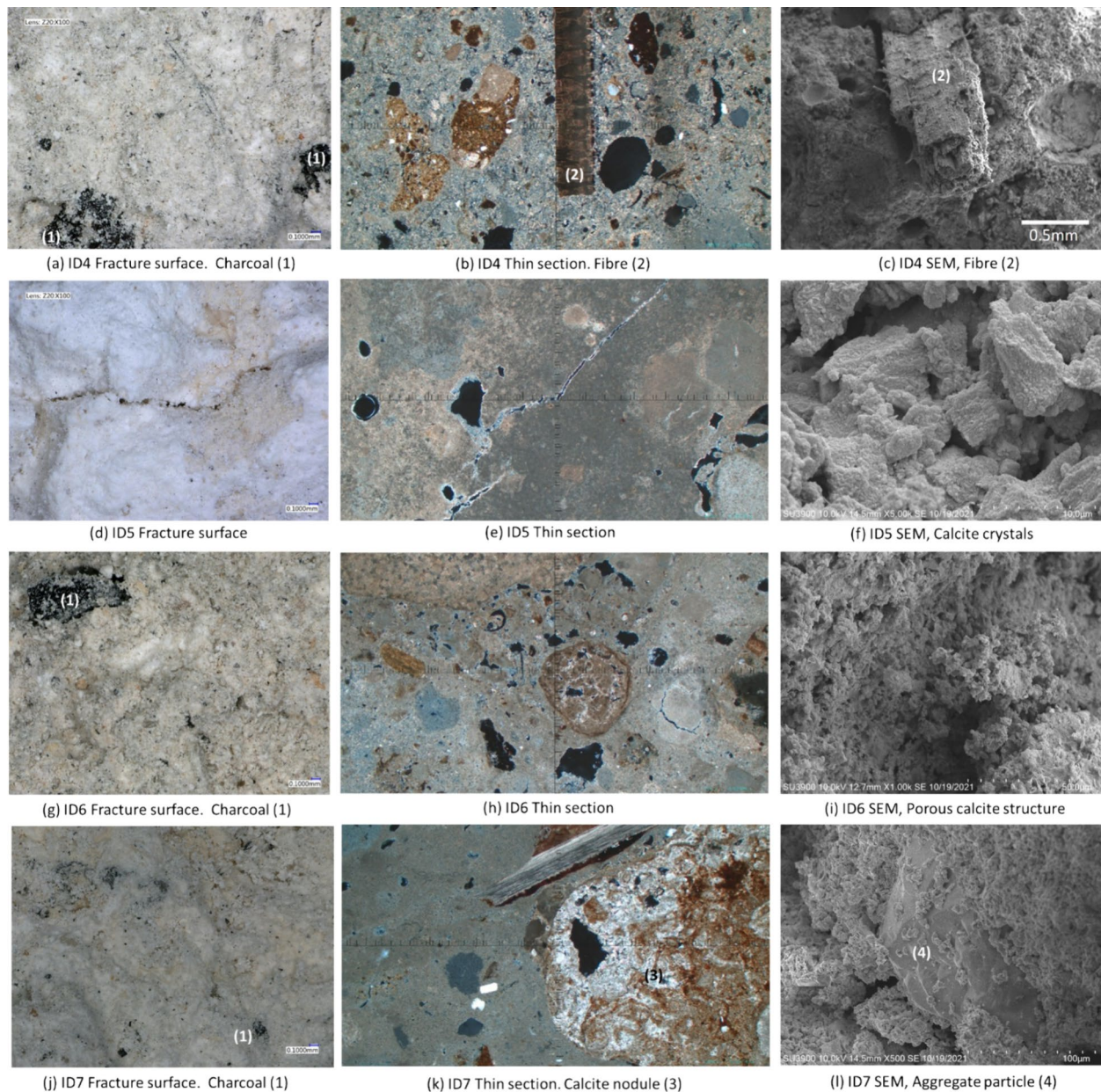


Fig. 5 Microscopy images of the samples from trenches P (ID4 and ID5) and V (ID6 and ID7): **a** Optical microscopy image of ID4 fracture surface with black charcoal particles (1); **b** ID4 transmission polarised image showing a range of different sized and mineralogical aggregates including organic fibre section (2); **c** SEM image of organic fibre extruding from the mortar structure; **d** Optical microscope image of ID5 showing white calcite crystals and a horizontal crack; **e** Thin section polarised image of ID5 showing mortar and aggregates with crack; **f** SEM image of agglomerates of calcite crystals and internal porosity in ID5; **g** Optical microscope image of ID6 fracture surface showing grey granular structure with fine aggregates and charcoal particle (1); **h** Thin section image of ID6 showing aggregates of varying mineralogy and size; **i** SEM image of ID6 showing fine porous structure of calcite crystals; **j** Optical microscope image of ID7 showing distribution of small charcoal particles throughout mortar matrix; **k** Thin section polarised image of (ID7) showing mortar on left hand side, calcite nodule on right hand side, and cross-section of mineral phase and its internal layered structure in top middle; **l** SEM image of ID7 showing aggregate particle coated in fine calcite crystals. (1 unit on thin section images = 0.0267 mm)

with a much sparser layer of calcite crystals. This is a feature more specific to Byzantine practice.

Figure 5 presents microscopy images from the samples belonging to trenches P (ID4 and ID5) and V (ID6 and ID7). These mosaics originally decorated the upper floors of the Umayyad building referred to as the ‘House of the Tesserae’. The mortars have some similarities to the structures identified by Hamarneh and Abu-Jaber containing secondary overgrowth [40]. Figure 5a shows an optical microscopy image of the ID4 fracture surface with a white granular texture with black charcoal particles (5a.1). Figure 5b is a transmission polarised image of ID4 with a range of different sized and mineralogical aggregates including an organic fibre section (5b.2). Figure 5c is a SEM image which includes an organic fibre projecting from the mortar fracture surface (5c.2). The optical microscope image of ID5 in Fig. 5d has white calcite crystals and a horizontal crack. Figure 5e is a thin section polarised image of ID5 with mortar and aggregates visible and a crack at approximately 45 degrees. Figure 5f shows an SEM image of agglomerates of calcite crystals and the internal porosity of ID5. Figure 5g presents an optical microscope image of the ID6 fracture surface showing the grey granular structure with fine aggregates and charcoal particle (5 g.1). Figure 5h is a thin section image of ID6 with aggregates of varying mineralogy and size. Figure 5i is a SEM image of ID6 with a fine porous structure of calcite crystals. Figure 5j presents an optical microscope image of ID7 showing the distribution of small charcoal particles throughout mortar matrix (5j.1). Figure 5k is a thin section polarised image of ID7 showing mortar on the left hand side and a large calcite nodule (5 k.3) on the right hand side [48]. The top middle of this image shows a cross-section of the mineral phase and its internal layered structure. Figure 5l is an SEM image of ID7 with an aggregate particle coated in fine calcite crystals (5 l.4). In summary, the mortars described exhibit

characteristics common to the Late Roman and Byzantine eras, but their unusual combination, along with the historical setting, could possibly indicate a distinctive Umayyad period identity.

Figure 6 shows the scanning electron microscope images of the polished cross sections of the red, creamy-white, and black tesserae. These come from trench S and relate to the Roman-period sample ID1. The polycrystalline structure of the tesserae is clearly visible.

Pore and aggregate distributions measured from optical images of thin sections

Frequency plots showing the size distributions of pores and aggregates in the mortars ID1 to ID7 are shown in Fig. 7a–g respectively. Data was obtained from measurements taken from optical images of polished thin sections. The Roman mortar ID1 (Fig. 7a) has noticeably larger aggregates, extending up to 1 mm, and pores compared to the other mortars. The late Roman mortars ID2 (Fig. 7b) and ID3 (Fig. 7c) contained similar pore size ranges to ID1 including finer pore sizes, however, sample ID3 did not have any aggregate particles. This is highly likely to be related to the effect of the hydraulic character of Byzantine mortars. ID4 (Fig. 7d) has even distributions of pores and aggregates with a high proportion of pores around 0.17 mm. ID5 (Fig. 7e) had a low proportion of aggregates 0.05–0.25 mm. A smaller concentration of aggregates might be indicative of a localized practice or resource availability during the Umayyad era. ID6, the most porous mortar, has well-proportioned pores (Fig. 7f) and ID7 had a wide range of aggregate sizes with pores at lower sizes but a greater number (Fig. 7g). The Umayyad period saw a fusion of styles and techniques from different periods and peoples. A mortar with a wide variety of aggregate sizes may signify a blend of building traditions, a hallmark of Umayyad architecture.

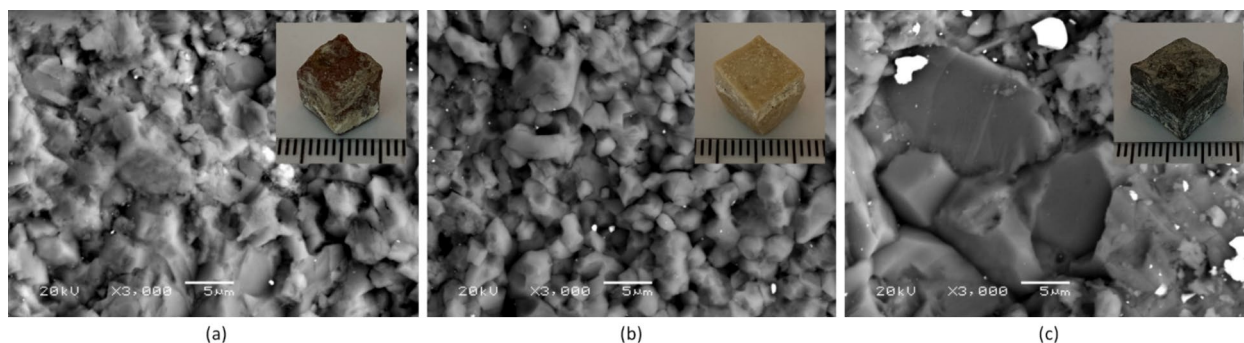


Fig. 6 Scanning electron microscopy images of polished surfaces of the **a** red, **b** creamy-white and **c** black tesserae from trench S. Insets show examples of the tesserae sectioned for polishing (scale divisions 1 mm). Bright white particles in the images are residual polishing media attached to the surface

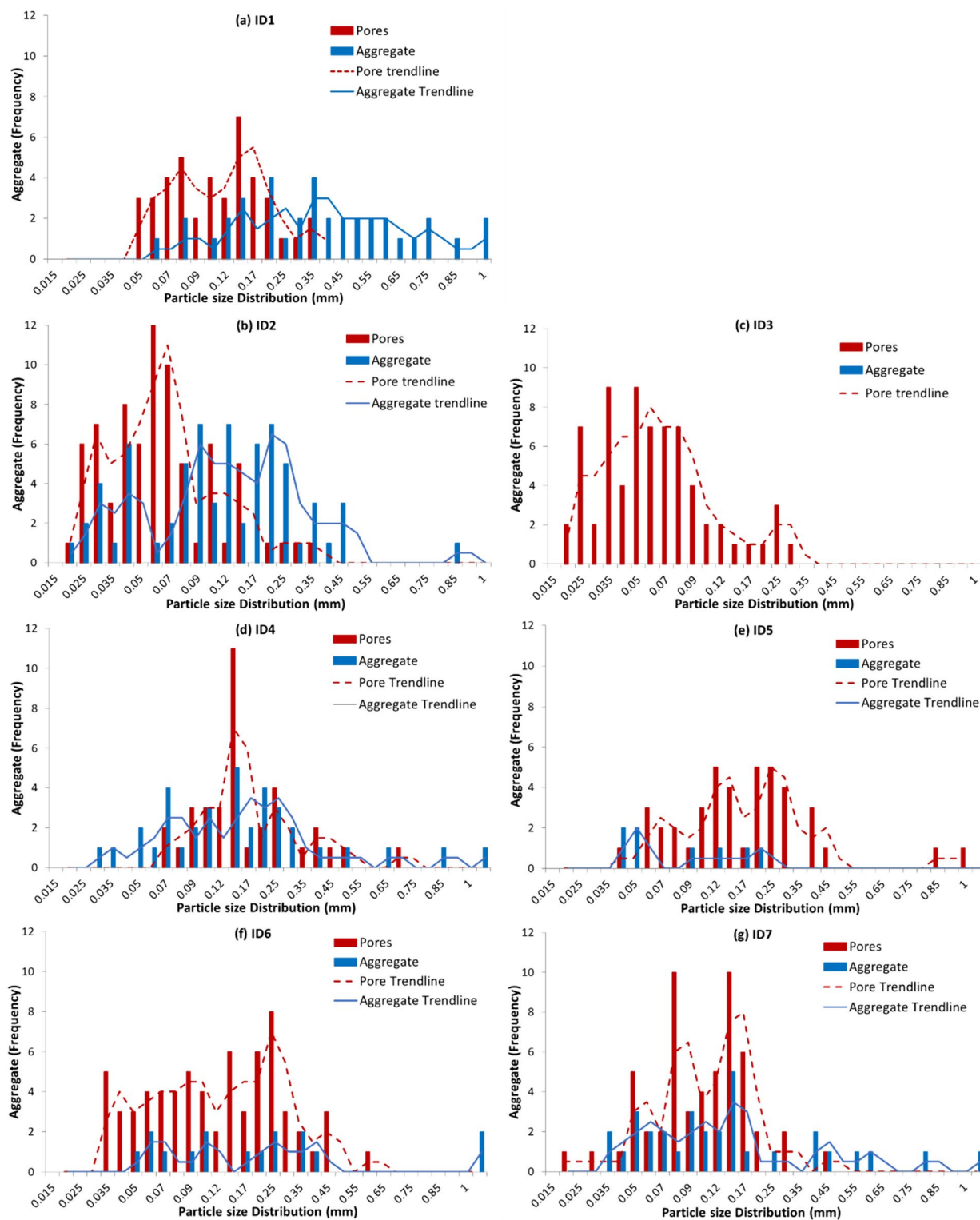


Fig. 7 Pore and aggregate size distributions obtained from measurements taken from optical images of polished thin sections for samples ID1b to ID7

Binder to aggregate ratio as a percentage for mortar and grout samples

The binder to aggregate ratio, as a percentage, was obtained gravimetrically following extraction by acid dissolution. Figure 8 shows that aggregate ratios in the adhesives were 4% and 6% for Roman (ID1a), and late Roman and Byzantine (ID3a) adhesives respectively. The

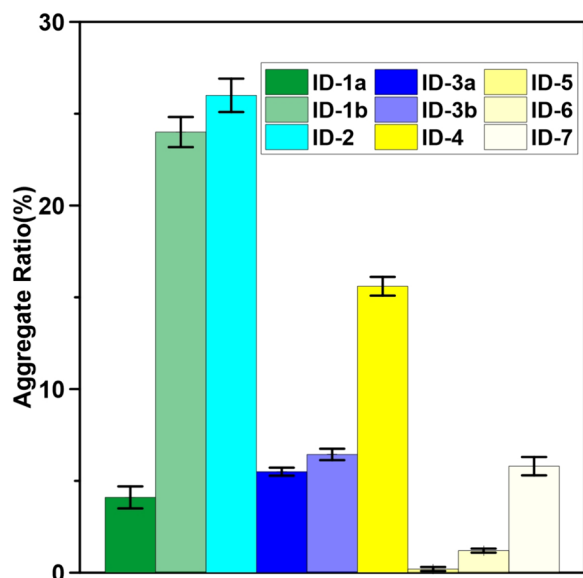


Fig. 8 Aggregate to binder ratios obtained gravimetrically for samples ID1 to ID7

mortars show a much higher variation in the aggregate content from <1% for the Umayyad mortar (ID5) to 26% for the late Roman and Byzantine mortar (ID2) which had the highest aggregate ratio. Although caution should be exercised due to sample size, the results suggest that the Roman and Umayyad adhesives had much reduced aggregate quantities for their adhesives (Table 1).

Mercury intrusion porosimetry (MIP)

The pore size distribution of the mortar specimens, and also the grout/adhesive ratio in the case of specimen ID1 from trench S, were determined using mercury intrusion porosimetry. Pore sizes were measured in the range from 3 nm to 1×10^5 nm (100 μ m) and are shown in Fig. 9. The total porosities by mercury intrusion for the specimens tested are presented in Table 2. Porosities ranged from 41.59 to 56.63% for the mortars, however, the porosity of the adhesive of the Roman mosaic from trench S showed a lower value of 30.90%. These mortar porosities are comparable with those measured in Roman mortars from Campania, southern Italy, where pore radii between 5 and 100 nm and open porosities of 39.9% and 52.4% were reported [49]. In an earlier study by Rispoli on the pozzolanic mortars from the thermal complex at Baiae, the typical pore radii ranged from 5 to 100 nm, although one sample contained larger pores ranging from 100 to 1000 nm [41]. In these mortars the open porosity was between 38.2% and 49.9% by volume. Both these studies showed an unimodal and broadened shape of the

Table 1 Details of the specimens collected and studied from trenches excavated by the Northwest Quarter Project

Preservation name		Location			Chronology	
ID	Find number	Trench	Context	Function	Date	
ID1	Find number: J16-Sa-1-44 MR16	S	A modern fill (topsoil) with ancient at lower level	Mosaic fragment associated with those from within the cistern	ID1a=adhesive, ID1b=mortar	Roman (R)
ID2	Find number: J15-Og-52-1 PL58	O	A fill of early Byzantine date with mosaic fragments in a secondary context	Associated with trench X and ID3	Mortar	Late Roman and Byzantine (LR/B)
ID3	Find number: J16-Xb-2-280 MR110	X	A mixed fill with mosaic fragments in a secondary context	Associated with trench O and ID2	ID3a=adhesive, ID3b=mortar	
ID4	Find number: J15-Pb-16-154 PL73	P	A mixed fill from the upper-storey collapse with mosaic fragments (including ID5)	Associated with trench V (ID6, ID7)	Mortar	Umayyad (U)
ID5	Find number: J15-Pcd-13-3 PL3	P	A mixed fill from the upper-storey collapse with mosaic fragments (including ID4)	Associated with trench V (ID6, ID7)	Mortar	
ID6	Find number: J16-Vdf-25-43 MR13	V	A mixed fill from the upper-storey collapse with mosaic fragments (including ID7)	Associated with trench P (ID4, ID5)	Mortar	
ID7	Find number: J16-Vi-26-26 PL37	V	A mixed fill from the upper-storey collapse with mosaic fragments (including ID6)	Associated with trench P (ID4, ID5)	Mortar	

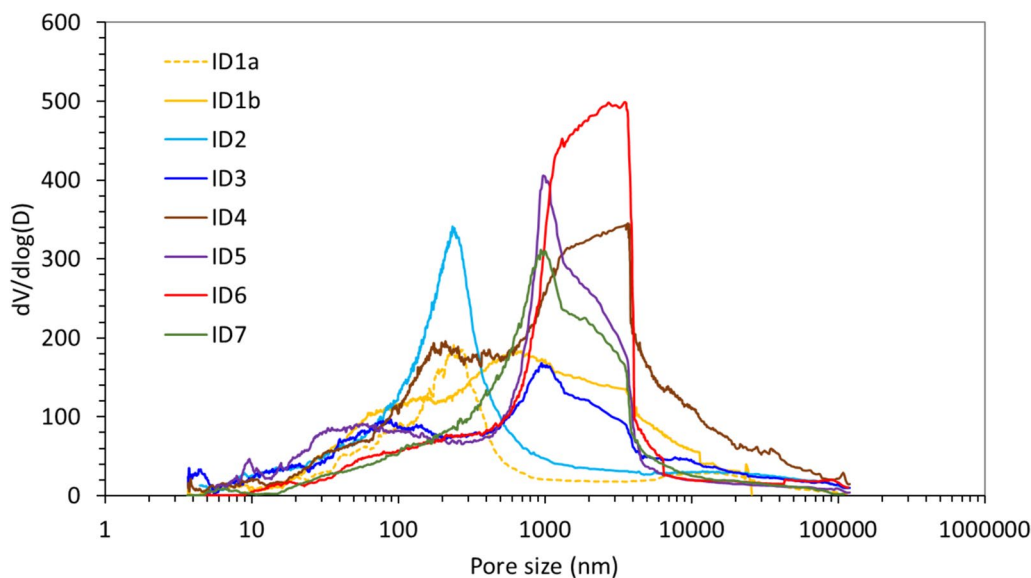


Fig. 9 Pore volume distribution obtained by mercury intrusion porosimetry for mortar samples

Table 2 Total porosity by mercury intrusion

ID	Trench	Date	Total porosity by mercury intrusion (%)
ID1b (mortar)	S	R	47.07
ID1a (adhesive)	S	R	30.90
ID2	O	LR/B	43.91
ID3	X	LR/B	41.59
ID4	P	U	56.63
ID5	P	U	45.53
ID6	V	U	52.16
ID7	V	U	44.81

R Roman, LR/B late Roman/Byzantine, U Umayyad

cumulative pore size distribution. Interestingly, the mortars we present here show a roughly bimodal distribution of pore sizes with peaks centred at approximately 200 nm and 2000 nm. The relative proportion of these two pore sizes varied between the samples as shown in Fig. 9. ID2, Roman period mortar showed a broadening of the cumulative pore size distribution, while ID3 became distinctive with a unimodal pore distribution with the peak at around 200 nm which is consistent with higher strength as reflected by the structural integrity. For ID4–ID7, the broadened shape distribution could be indicative of the various architectural forms observed during the Umayyad period being a combination of different styles.

A comprehensive study of the pore size distributions of several different formulations of lime mortars has been reported by Figueiredo [50]. Pure lime (CL90)—CL stands for Calcium Lime and 90 is minimum 90%

calcium hydroxide—mortars were compared to cement/lime hybrid mortars and lime/metakaolin mortars. The mortars with greater proportions of hydraulic compounds exhibited a single modal distribution which became less prevalent in mortars with higher proportions of lime showing a bimodal distribution. This supports the observational differences between the mortars of sites in southern Italy, where pozzolanic materials are well known, and Jerash. Pure limes tended to have larger pores with the porosity by intrusion in CL90 and lime putty being 30.47% and 34.45% respectively, compared to porosities ranging from 25.19% and 34.93% in the hydraulic mortars [51]. The pore size distribution is expected to influence the flow of moisture through the material thus determining its moisture content and drying times. Carbonation requires the presence of moisture and carbon dioxide which diffuse through the material. It therefore follows that a porous mortar may have carbonated and hardened more rapidly during its early life [52, 53].

Energy dispersive X-ray analysis (EDX)

EDX analysis of mortars

The elemental composition of the mortars was determined by energy dispersive X-ray analysis on samples of mortar and adhesive from trench S (ID1a and ID1b) and trench X (ID3a and ID3b) and mortar only from trench P (ID4). These are shown in Table 3. The slightly lower Carbon (C) content is consistent with the use of non-hydraulic lime in mortars, as observed in Roman Period for ID1. The most abundant elements identified were C, O, Mg, Al, Si and Ca, with a trace amount of P found in ID4. The

Table 3 Energy dispersive analysis of X-rays (EDX) analysis of mortar samples which cover the complete chronology in this study showing the atomic % elemental composition

ID	ID1a	ID1b	ID3a	ID3b	ID4
Trench	S	S	X	X	P
Element	Adhesive	Mortar	Grout/adhesive	Mortar	Mortar
C	19.9	20.0	21.9	23.8	26.7
O	43.2	46.9	29.4	47.1	42.6
Mg	0.4	1.4	1.4	2.1	0.7
Al	0.3	0.8	1.5	1.1	0.7
Si	0.4	2.5	2.8	3.0	3.4
P					0.6
Ca	35.7	28.5	43.1	22.9	25.3

more diversified pattern observed in ID4 serves as an indicator of mortars from the Umayyad period. C, O and Ca can be attributed to the calcite phase of the lime mortar and the Si to the presence of small quantities of quartz which is often found in limestone [54]. This observation is supported by phase analysis carried out using X-ray diffraction and Raman spectroscopy. The relatively small quantities of Mg, Al and P are likely to originate from additional mineral phases that were present in the limestone used to manufacture the mortar or any fine aggregate additions. Although the use of volcanic and other materials as pozzolanic additions in Roman mortars is widely reported, our results suggest that the mortars in this study are non-hydraulic in nature [55, 56].

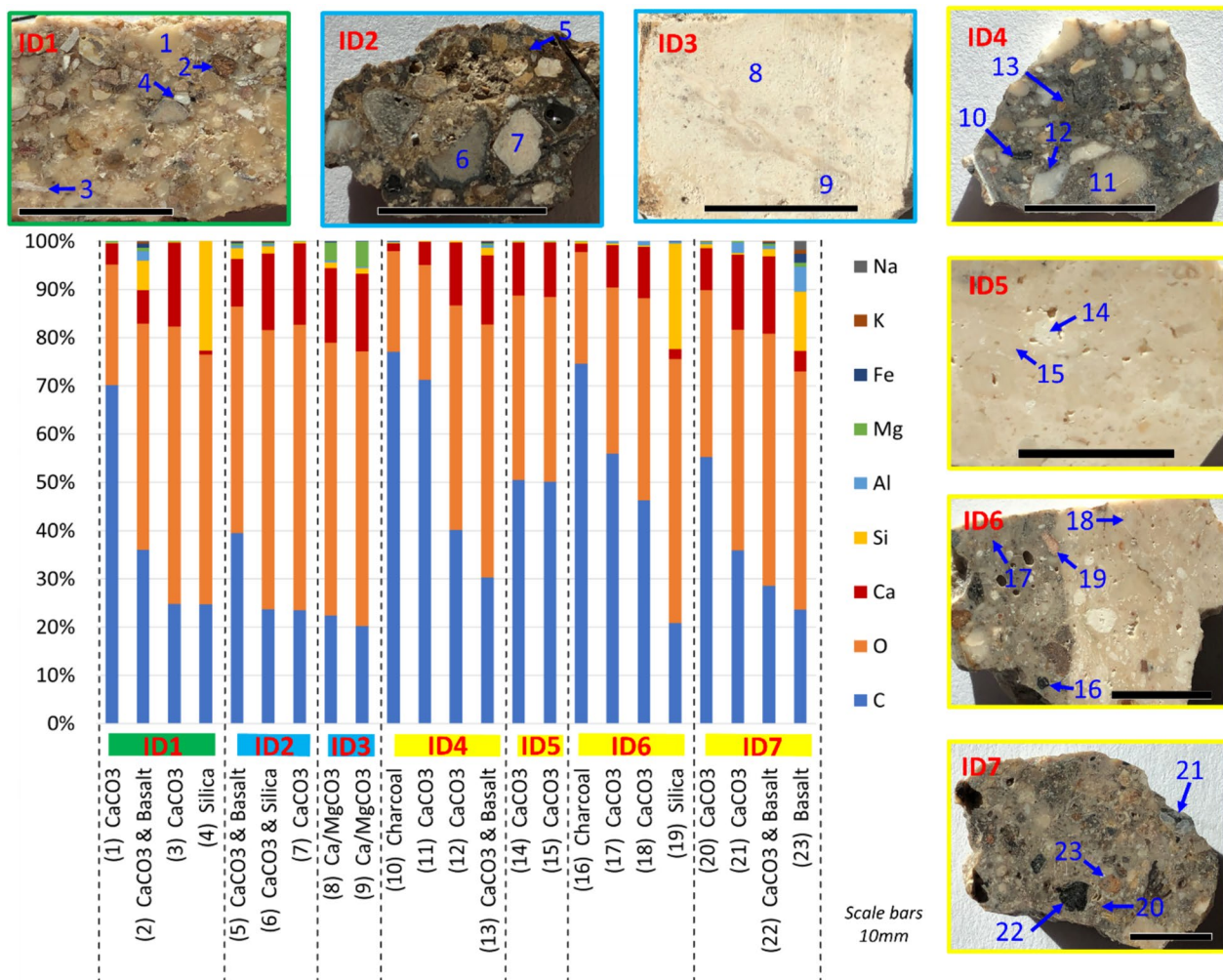


Fig. 10 Energy dispersive analysis of X-rays (EDX) semiquantitative analysis of aggregates within mortar samples for carbon (C), oxygen (O), calcium (Ca), silicon (Si), aluminium (Al), magnesium (Mg), iron (Fe), potassium (K) and sodium (Na). Presented in the form of a stacked column chart in atomic %. Aggregate locations are shown in photographs

EDX analysis of aggregates in mortars

A detailed analysis of the composition of aggregate phases in the mortar samples is presented in Fig. 10. The figure shows images of mortar sections that were impregnated with resin and then cut using a diamond saw. Between 2 and 4 aggregates from each specimen were analysed and the relative composition in atomic % for the elements carbon (C), oxygen (O), calcium (Ca), silicon (Si), aluminium (Al), magnesium (Mg), iron (Fe), potassium (K) and sodium (Na) is presented as a stacked column chart. It should be noted that carbon values may be higher than expected due to beam skirt under the low vacuum. The Roman mortar (ID1) contained a mixture of different aggregate types consisting of calcium carbonate, silica and clay which could be an indication of marly limestone. The Late Roman and Byzantine mortars (ID2–3) have a similar composition, however, ID3 contained a noticeable magnesium content which would be consistent with the use of a dolomitic lime. It is noteworthy that this is the only sample in which aggregates were not observed and therefore the result is likely to correspond to the mortar. The composition of early Islamic mortars is shown in ID4–7. The most noticeable difference between mortars from this period and the earlier Roman mortars is the evidence of large charcoal particles, Figs. 4b, 5a and g. The later mortars contained the highest proportions of carbon and were black in colour. The aggregates in the mortars from all periods contained of the elements Al, Mg, Fe, K and Na. These elements are characteristics of basalt which was positively identified in a thin section image from sample ID1 (see Fig. 3b.1).

EDX analysis of tesserae from sample ID1

Elemental analysis was also performed for the white, grey, and red tesserae from ID1, which is reported in

Table 4 EDX analysis of white, grey, and red tesserae removed from ID1 showing the atomic % elemental composition

Element	Colour		
	White	Grey	Red
C	15.0	15.7	15.6
Mg	0.1	0.1	0.2
Al			0.2
Si	0.4	0.1	0.4
Ca	35.5	34.6	31.1
Fe			1.4
O	48.9	49.5	51.0

Table 4. All the tesserae contained C, Mg, Si, Ca and O, with Al observed in the red tesserae.

A comparison of the elemental composition between the tesserae and mortars indicates small traces of Al present in all the mortars, however Al was only detected in the red tesserae. This suggests that the stone used for the white and grey tesserae could not have been the same as that used to manufacture the mortar. Using a similar reasoning the presence of Fe in the red tesserae, and its absence in any of the mortars, suggests that the mortars were not manufactured from the stone used for the red tesserae. This indicates, therefore, that the stone used for each of the three coloured tesserae and that for the mortar from trench S all came from different sources. Hamarneh and Abu-Jaber, and also Thomsen, have reported that the lime mortars from Jerash were manufactured from locally sourced limestone [40, 57]. Our results indicate, therefore, that a range of sources, whether at a local or regional level, were exploited for the tesserae and the lime. This observation needs to be determined for the later periods to produce a more comprehensive history.

Thermogravimetric analysis (TGA)

Figure 11a, b show the TG and dTG curves plotted from the thermogravimetric analysis data. A small weight loss up to 200 °C, Fig. 11a, is related to the desorption of water adsorbed onto the surface of the sample. Most of the weight loss occurs between 650 and 800 °C and is attributed to the decarboxylation of calcium carbonate, Fig. 11b. The calcium carbonate content, as a percentage, was calculated for each sample using the stoichiometric ratio and is presented in the legend.

X-Ray diffraction (XRD)

Figure 12a shows X-ray diffraction patterns obtained from the specimens in the 2-theta range 5 to 60 degrees. Major peaks corresponding to the phases quartz and calcite were matched with PDF data files #78-1252 and #05-0586 respectively. All specimens contained both calcite and quartz, however, the relative amount of these two phases varied with some samples containing higher proportions of quartz compared to others. The results did not suggest any consistent trend between the amount of quartz and the trench from which the sample was taken.

XRD of the residue remaining following acid dissolution, Fig. 12b, identified the presence of quartz which agreed with the analysis of the mortars. In the case of samples ID1 and ID2 it was possible to easily isolate aggregates of different colours, either 'brown' or 'white', however in both cases the dominant phase remained quartz. Since the calcium carbonate binder had been dissolved away, the clay illite was identified in samples ID3a,

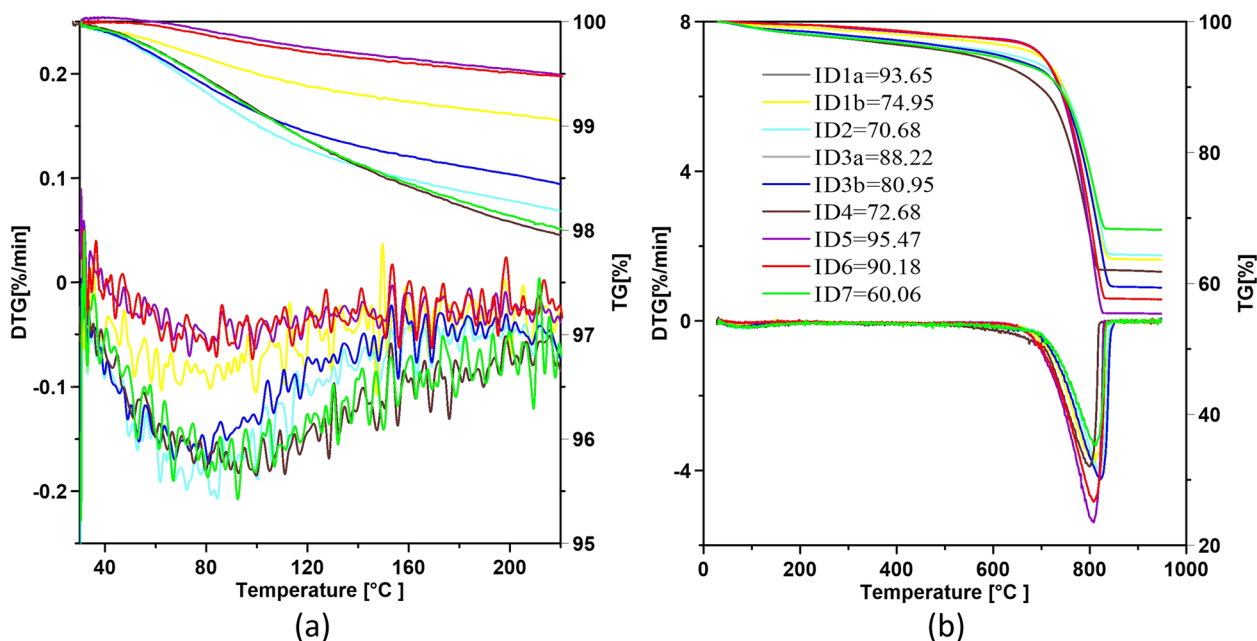


Fig. 11 Thermogravimetric analysis obtained from mortar samples. Legend shows calculated percentage calcite

ID3b, ID4, ID5 and ID7. There are reports of illite and other clays being used as pozzolanic materials [58], however, as the XRD signal was extremely low and it was not detected by the other techniques it may have been present as a result of contamination in the sand, or during mixing, rather than being added intentionally.

Fourier transform infrared spectroscopy

The chemical bonds in historic mortar and grout were assessed using FTIR analyses. Spectra obtained for the mortars are shown in Fig. 13. The strong adsorption bands demonstrated the presence of carbonates in the samples by the assignment of peaks of wavenumbers 1790 and 1820 cm^{-1} ; 1400 and 1500 cm^{-1} ; and at 868 cm^{-1} and 710 cm^{-1} [59]. The IR bands at 711 cm^{-1} (ν_4 : in-plane bending) and 873 cm^{-1} (ν_2 : O–C–O out-of-plane bending) correspond to the characteristic bonds of calcite. The strong band at 1402 cm^{-1} is attributed to the symmetric stretching vibration of CO_3^{2-} ions, and the weak band at 1797 cm^{-1} corresponds to $\nu_1 + \nu_4$ symmetric CO_3^{2-} ions [60–62]. The double peak centered at around 776–796 cm^{-1} confirmed the presence of quartz, and the band centered at 1031 cm^{-1} is attributed to the Si–O stretching band [63–65].

Raman spectroscopy

A series of Raman spectra were obtained for several of the samples with mortar and adhesive. Some spectra exhibited a high background fluorescence which dominated the signal masking any underlying peaks from the

structure; these spectra are therefore not included. Figure 14 shows representative spectra where the peaks could be resolved easily. Vibrational modes of the free CO_3^{2-} ion, A_{1g} are visible at 1085 cm^{-1} and E_g modes were located at 717, 286 and 157 cm^{-1} respectively. Of these, the A_{1g} active mode is the strongest by far [13]. These results are in agreement with TGA, FTIR, and XRD which also identified the presence of calcite.

Discussion

The results are discussed in chronological order starting with Roman, followed by Late Roman and Byzantine, and ending with Umayyad, Early Islamic.

Roman (63 BC—early fourth century AD)

The mosaic fragment from trench S (ID1a and ID1b) belongs to the only group of materials from the Northwest Quarter that can be attributed, with certainty, to the Roman period. They are also one of the few surviving examples of a Roman tessellated pavement from the city [18]. The decoration is quite simple, consisting of a white adjusting border, a creamy-white fillet, and then a geometric pattern, formed of triangles or diamonds [66]. The finish is, however, of high quality with small stone tesserae laid tightly together to form a flat surface. The tesserae in the decorative part were between 0.5–0.9 cm, with a tessera density of 120–130 per dm^2 , while those in the adjusting border are larger at 1.0–1.2 cm, with a density of 65–70 per dm^2 . It is the earliest known example from Jerash, dating to the late first

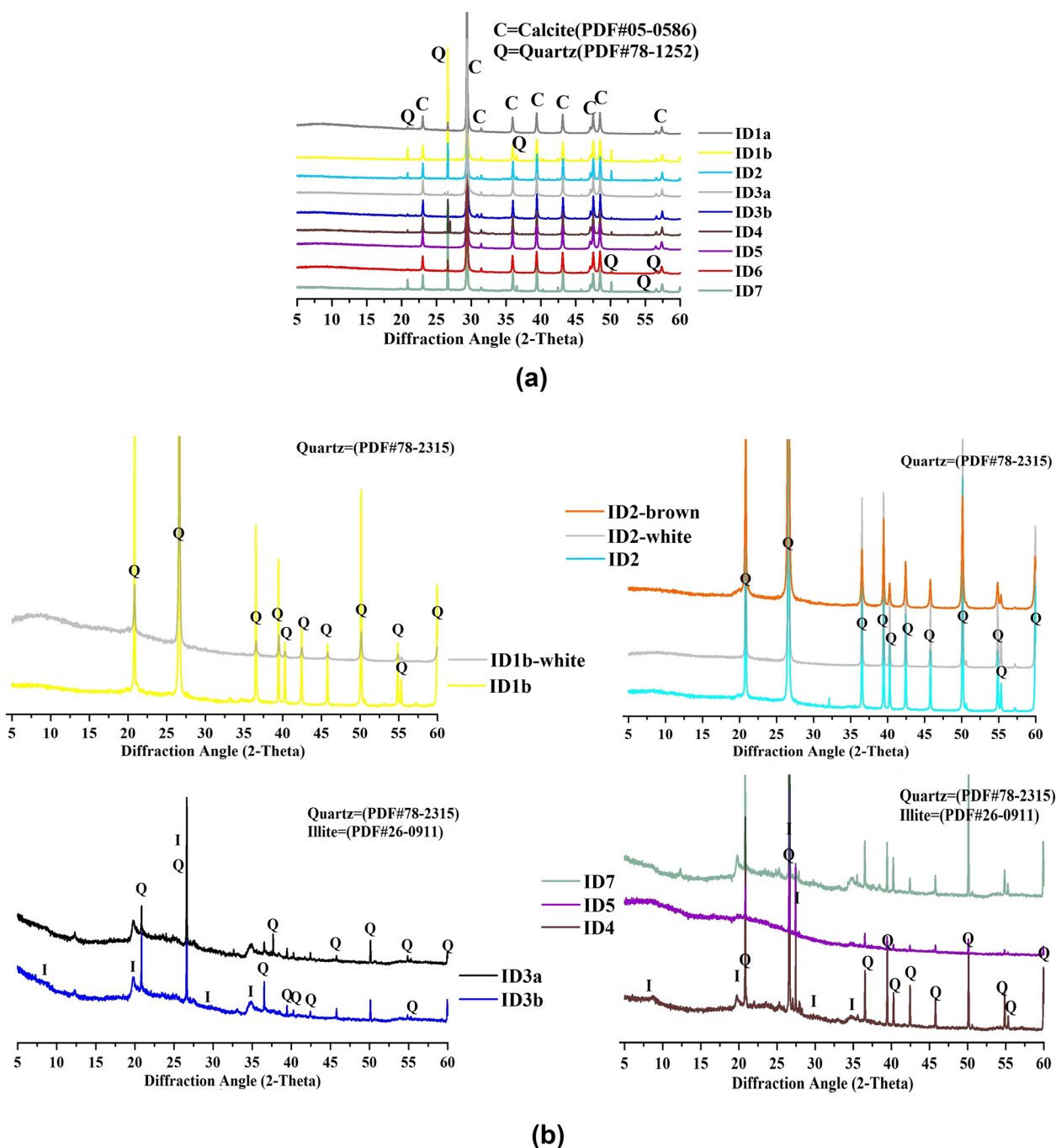


Fig. 12 X-ray diffraction patterns of **a** mortar samples showing the presence of calcite and quartz, **b** residues remaining after acid dissolution

or early second centuries AD, and also the simplest; the well-known Mosaic of the Muses, whose much-debated date sits somewhere in the second or third centuries, has a more complex figurative design and employs glass tesserae in addition to the stone [14, 21, 22, 67]. The analysis characterized the adhesive, or setting bed, and the mortar of one fragment from the decorative area.

All fragments from this mosaic had a similar two-layer bedding.

The mortar (ID1b) and adhesive (ID1a) were found to be different in composition. The adhesive had a higher lime content, finer structure (Fig. 9), and was less porous (Table 2). There were also differences in the composition supported by more intense peaks corresponding to

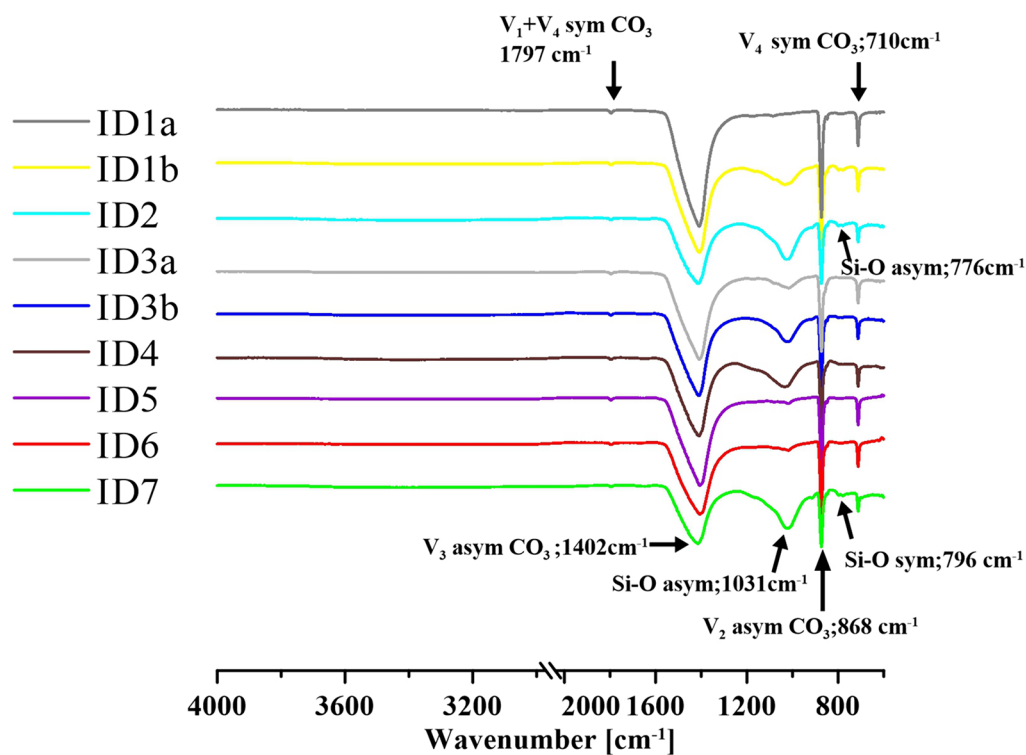


Fig. 13 Fourier transform infrared (FTIR) spectra obtained from mortar samples. *Sym* symmetrical, *asym* asymmetrical

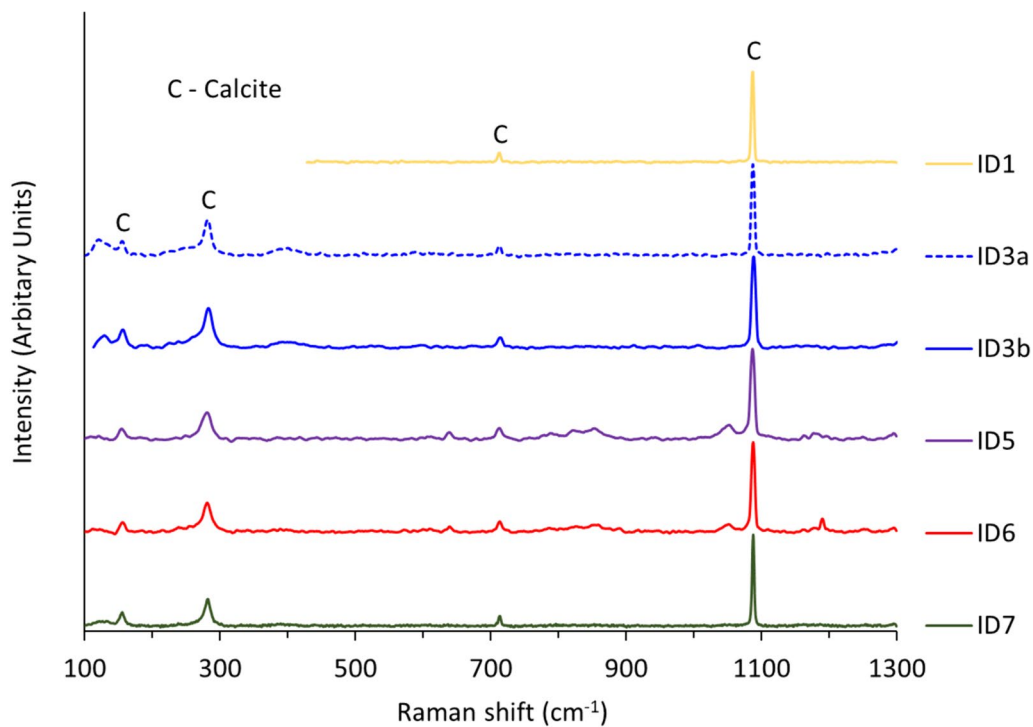


Fig. 14 Raman spectra obtained from mortar samples ID1, ID3a, ID3b, ID5, ID6 and ID7

quartz in the XRD pattern (Fig. 12) and FTIR spectra (Fig. 13). The mortar had larger aggregates in a range of materials while the adhesive contained natural fibres (Fig. 3d). Their small diameter and hollow structure can be identified as the individual xylem of a natural plant fibre; they are not animal hairs [68]. They are bast fibres which come, most likely, from flax, hemp, or straw, which were commonly grown in antiquity for textiles. The landscape around Gerasa, which has been called a 'garden city' [69], supported all major ancient crops, including cereals and oilseeds. Plant fibres were not only a readily-available source of aggregate but also had beneficial effects on the properties of the mortar, increasing their compressive and tensile strengths while improving fracture toughness [46, 47, 70, 71].

The materials were adjusted for the aggregate of the adhesive, adding plant fibres, and using no large quartz grains, and the binder had a higher lime content of 93.65% compared to 74.95% for the mortar (Fig. 11). This careful selection demonstrates the extra attention paid to the layer into which the tesserae were set. The observation is supported by the original context of this mosaic, which was likely a large, impressive, and highly-decorated building. This is the first time that mosaic mortars of Roman date have been studied at Gerasa and, therefore, provides an important insight into their composition and structure. The adhesive of this mosaic is the highest quality of all those analysed here while the mortar is more comparable with the later examples. It has also been shown that the sources of limestone for the lime were different from those used for the tesserae, suggesting planned exploitation of materials for different uses.

Late Roman and Byzantine (early fourth century AD—mid 7th century AD)

The mosaic fragments from trenches O and X (ID2 and ID3) were found in mixed fills associated with the remodelling of the terrace when Byzantine and Umayyad structures were built on top of an earlier Roman-period water management system including a cistern and sediment basin. Although the fragments belong to secondary contexts, the similarities in construction technique and surface decoration, which consists of elongated white limestone tesserae, suggests that they all come from the same pavement [66]. The similar macro porosity supports this proposal (Fig. 7). The original location of this mosaic pavement is unknown, and the date is sometime prior to deposition during the changes to the terrace. The sample from trench O only retains the mortar (ID2) but the one from trench X (ID3) retains the complete bedding sequence, as known, from the surface tesserae through the adhesive (or setting bed) to the mortar bedding.

Numerous offcuts, from the processing of limestone into tesserae, were found in the bedding used as an aggregate.

The lime from the samples from both trenches was identified by the TGA (Fig. 11), XRD (Fig. 12), FTIR (Fig. 13) and Raman spectroscopy (Fig. 14) as calcite, the same as that from all the other trenches. The fragment from trench X was the only one to be analysed with SEM–EDX but both the adhesive (ID3a) and the mortar (ID3b) were examined (Figs. 1, 8, 11, 12 and Table 3). The general observation is similar to the sample from trench S, the adhesive manifested a higher lime content than the mortar and also a lower aggregate content (Fig. 8). The actual quantity, however, is lower in trench X than the earlier Roman mosaic fragment (ID1b). The mortar contained fibres resembling those from plant fibres and small pieces of carbonised wood (Fig. 4b, c, f, j). The presence of burnt and unburnt organic debris, including charcoal, in the mortars of the Northwest Quarter has been previously reported [1, 57]. These observations are consistent with other research, where wood has been noted as a fuel to calcine limestone for the production of lime [40]. It is likely that the charcoal was not added intentionally to the mortar but rather is residual, trapped during the slaking process after the limestone was burnt in a kiln. Lime kilns are known close to Jerash and the surrounding area [40], and also in the city where, for example, in the Macellum a small lime kiln was built in the sixth century [72]. The lime produced in the latter was slaked locally and used in the building renovations and another kiln has been identified near the Church of St Theodore [72].

The SEM–EDX shows that the mortar sample from trench X is more porous than the adhesive. This indicates extra effort being put into the mixing of the setting bed, similar to that observed in trench S. The overall porosity of the specimens from trenches O and X lies between the results for the adhesive and mortar from trench S. This now-fragmentary pavement is thought to have had a more functional purpose in its original context due to the use of elongated tesserae. All the analyses, however, show care was taken during preparation, using lime with different purity levels, and making small adjustments to the aggregate. They are comparable in approach and materials to the earlier Roman mosaic floor even if the adhesive from trench S was of higher quality.

Umayyad, Early Islamic (seventh century AD to 749 AD earthquake)

The samples from trenches P (ID4 and ID5) and V (ID6 and ID7) formed part of the mosaic decoration of the upper floors of an Umayyad building, the so-called 'House of the Tesserae', which was destroyed in an earthquake in January of 749 AD. The impressive property, constructed in the early eighth century around a

courtyard, received its name from a trough containing thousands of unused tesserae, which were probably being stored following renovation [35, 66]. It is not known whether the fragments come from a single pavement or a series of rooms belonging to the first floor of the property. The range of porosities may suggest the latter.

Lime content determined by TGA (Fig. 11) show that the mortars from trench P (ID4 and ID5) had lime contents of 72.68% and 95.47% respectively. In comparison, mortars from trench V had lime contents of 90.18% and 60.06% respectively. On average trench V has lower lime content than the samples from trench P. Compared to trench S (ID1) which had a lime content of 93.65%, these were on average lower. Trenches O (ID2) and X (ID3) had lime contents of 70.88% and 80.95% respectively, indicating values lower than trench S and comparable to trenches P and V. The XRD (Fig. 12) and FTIR (Fig. 13) results indicate that the samples from P and V have similar composition to the mortars from all the other trenches (S, O and X) suggesting that the basic characteristics remained relatively homogenous throughout the life of the quarter. It is noteworthy that higher intensity quartz peaks were observed in XRD and FTIR from ID7, ID4, ID3b, ID2 and ID1b. Like the other samples, there are slight differences in the aggregate with quartz sand grains, natural fibres and carbonised wood visible under magnification. The mortar structure and the aggregate contributed to the larger pore sizes and their higher number (Fig. 7). It seems quite likely that the mortars in both trenches P and V were prepared intentionally in this way according to the installation context as part of an upper floor. Even though the characterization shows similarities going back to the early Roman period, therefore, there are identifiable adjustments being made according to the location in which they were to be used. Furthermore, the appearance of wood in the mortar makes another connection to the process used to produce lime, as observed in trench X (ID3).

Conclusions

The following conclusions can be drawn from the investigations of the Roman, Late Roman and Byzantine, and Early Islamic mortars excavated from the Jerash North-west Quarter.

The composition and characteristics of the bedding mortars remained similar over the approximate 600-year life of the site, with the XRD, TGA, FTIR and Raman spectroscopy providing evidence indicating the presence of carbonate phases (calcite). None of the techniques used to analyse the mortars suggest the presence of hydraulic phases, and it is therefore proposed that the mortars are non-hydraulic. Optical microscopy investigations indicated the presence of black charcoal fragments

in the late Roman and Byzantine mortars, and Islamic mortars suggesting that wood was used as a fuel when preparing the lime (trenches X and P). In addition, elemental analysis of three different coloured tesserae from the surface decoration of the samples shows that different stone sources were used for lime and tesserae.

It was possible to separate samples of mortar and adhesive of the Roman-period mortar (trench S). MIP analysis revealed that the adhesive had a much lower porosity (30.90%) when compared to the other samples of mortar which have porosities ranging from 41.59 to 56.63%. EDX elemental analysis carried out on adhesive and mortar from trenches X and S both showed higher intensity signals for calcium in the adhesive (setting bed) when compared to the mortar. This is consistent with the lower porosity, and lower aggregate contents of the adhesives that were determined by acid dissolution, and higher lime contents determined by TGA. This attests to the differentiation between the bedding layers as well as the higher quality of the mortars prepared for this particular floor during the early Roman period.

Electron microscopy, and optical microscopy of Roman, late Roman/Byzantine and Umayyad mortars showed evidence of natural fibres, most likely flax, hemp or straw in the mortars. The aggregates in the mortars were characterised using optical microscopy of thin sections and elemental EDX analysis. The elemental composition of the aggregates indicated that most aggregates were calcite based with a small proportion containing significant proportions of silica. The presence of other elements in smaller concentrations such as Al, Mg, Fe, K and Na suggested that other mineral phases were present. XRD of the aggregate particles remaining after acid dissolution indicated quartz with small traces of illite. Aggregate particles visible in the polished thin sections, and viewed under polarised light, strongly suggested that basalt, amphibole may be present in Roman mortars and olivine in Late Roman and Byzantine mortars.

The various analyses demonstrate a long tradition of mortar production which was adjusted specifically for use in mosaics with further adaption to the specific layer of the bedding within the foundations. The approach remained similar over the course of the six centuries which these samples attest to but with some modifications, again depending on the location or function of the floors. The local landscape was exploited for the materials, including separate stone sources for the surface and lime as well as for the bast fibres. The latter were used to modify the mechanical properties, improving flexural and tensile strength while also reducing cost. The results offer further information about the lime production through the charcoal which attests to the burning of the limestone. This was found in nearly all the samples except for the earliest

Roman phase, which might suggest the use of a different, noticeably, higher quality batches of mortar. This fits well to the overall high quality of the house's interior decoration and inventory found associated with the mosaic fragments in the cistern. In addition to the significant new data on the historic production and use of mortars at Jerash, this paper also offers a clear methodology for the analysis and characterisation of mortars that will be of value to the wider scientific community.

Acknowledgements

The authors would like to thank the Carlsberg Foundation, Danish National Research Foundation (DNRF119), Deutsche Forschungsgemeinschaft, Deutscher Palästina-Verein, H. P. Hjerl Hansens Fond for Palästina Forskning, EliteForsk initiative of the Danish Ministry of Higher Education and Science, the H. P. Hjerl Hansens Mindefondet for Dansk Palästinaforskning. Thanks are extended to Diana Lednitzky for obtaining the Raman spectra, Gabriele Kociok-Köhn for X-ray diffraction experiments, Nasser Chakkiwala for optical microscopy, Olivier Camus for MIP and TGA analysis, Judith Brown for assisting with acid dissolution, and Claudia Hildebrandt (University of Bristol) for help with imaging of thin sections.

Author contributions

Richard J. Ball: conceptualization, methodology, formal analysis, investigation, resources, writing—original draft, writing—review & editing, visualization, supervision, project administration. Martin P Ansell: conceptualization, methodology, formal analysis, investigation, writing—original draft, writing—review & editing, visualization. Tugce Busra Su: methodology, investigation, writing—original draft, writing—review & editing, visualization. Vahiddin Alperen Baki: investigation, writing—original draft, writing—review & editing, visualization. Philip J. Fletcher: investigation, writing—review & editing. Achim Lichtenberger: conceptualization, writing—review & editing, project administration, funding acquisition. Rubina Raja: conceptualization, writing—review & editing, project administration, funding acquisition. Will Wootton: conceptualization, writing—original draft, writing—review & editing, visualization, project administration, funding acquisition.

Funding

Carlsberg Foundation, Danish National Research Foundation (DNRF119), Deutsche Forschungsgemeinschaft, Deutscher Palästina-Verein, H. P. Hjerl Hansens Fond for Palästina Forskning, EliteForsk initiative of the Danish Ministry of Higher Education and Science, the H. P. Hjerl Hansens Mindefondet for Dansk Palästinaforskning.

Availability of data and materials

Data included in the manuscript was collected by the authors in their laboratory. Where available, raw data can be made available upon request.

Declarations

Ethics approval and consent to participate

The research has received ethical approval from the University of Bath. It is noteworthy that the study has not included any human or animal studies.

Competing interests

The authors declare no competing interests.

Received: 7 December 2023 Accepted: 12 May 2024

Published online: 24 May 2024

References

- Lichtenberger A, Lindroos A, Raja R, Heinemeier J. Radiocarbon analysis of mortar from Roman and Byzantine water management installations

- in the Northwest Quarter of Jerash, Jordan. *J Archaeol Sci Rep.* 2015;2:114–27.
- Daugbjerg TS, Lichtenberger A, Lindroos A, Raja R, Olsen J. Revisiting radiocarbon dating of lime mortar and lime plaster from Jerash in Jordan: sample preparation by stepwise injection of diluted phosphoric acid. *J Archaeol Sci Rep.* 2022;41:103244.
- Lichtenberger A, Raja R. Late Hellenistic and Roman antioch on the chryso-rhoas, also called Gerasa: a reappraisal of the evidence in the light of the findings of the Danish–German Jerash northwest quarter project (2011–2017). In: Lichtenberger A, Raja R, editors. *Hellenistic and Roman antiochia on the chryso-rhoas, the former Gerasa: contributions on the archaeology and history of a Decapolis City.* Turnhout: Brepols; 2020. p. 7–54.
- Raja R. The sanctuary of artemis in Gerasa. In: Fischer-Hansen T, Poulsen B, editors. *From artemis to Diana: the goddess of man and beast.* Copenhagen: Museum Tusulanum; 2009. p. 383–401.
- Lichtenberger A, Raja R. Defining borders: the umayyad-abbasid transition and the earthquake of ad 749 in Jerash. In: Lichtenberger A, Raja R, editors. *Byzantine and Umayyad Jerash reconsidered transitions, transformations, continuities.* Turnhout: Brepols; 2019. p. 265–86.
- Raja R. Urban development and regional identity in the eastern Roman provinces, 50 BC–AD 250: aphrodisias, Ephesos, Athens, Gerasa. Copenhagen: Museum Tusulanum Press; 2012.
- Lichtenberger A, Raja R. Middle Islamic Jerash (9th century–15th century): archaeology and history of an Ayyubid–Mamluk settlement. Turnhout: Brepols; 2018.
- Lichtenberger A, Raja R. Middle Islamic Jerash through the lens of the longue durée. In: Lichtenberger A, Raja R, editors. *Middle Islamic Jerash (9th – 15th century) archaeology and history of an Ayyubid–Mamluk settlement.* Jerash Papers 3. Turnhout: Brepols; 2018.
- Lichtenberger A, Raja R. Ğeraš in the middle Islamic period: connecting texts and archaeology through new evidence from the northwest quarter. *Zeitschrift des Deutschen Palästina-Vereins.* 2016;132:63–81.
- Crowfoot D. The crystal structure of insulin I. The investigation of air-dried insulin crystals. *Proc R Soc Lond Ser A-Math Phys Sci.* 1938;164:580–602.
- Biebel, F. M. Mosaics. In *Gerasa, City of the Decapolis, an account embodying the record of a joint excavation conducted by Yale University and the British School of Archaeology in Jerusalem (1928–1930), and Yale University and the American Schools of Oriental Research (1930–1931),* (ed. Kraeling, C. H.). 294–354 (American Schools of Oriental Research, 1939).
- Lichtenberger A, Raja R. Mosaicists at work: the organisation of mosaic production in Early Islamic Jerash. *Antiquity.* 2017;91:998–1010.
- Boschetti C, Lichtenberger A, Raja R, Wootton W, Schibille N. Loose glass tesserae and lost decorations: chronology and production of mosaics from Gerasa's Northwest Quarter*. *Archaeometry.* 2021;63:960–74.
- Piccirillo M, Bikai PM, Dailey TA. *The mosaics of Jordan.* (vol. 1). New Haven, Conn: American center of Oriental research Amman; 1993.
- Balty J. *Mosaïques antiques du Proche-Orient: chronologie, iconographie, interpretation.* vol. 551. Besançon: Presses Univ. Franche-Comté; 1995.
- Michel A. *Les églises d'époque byzantine et umayyade de Jordanie (provinces d'Arabie et de Palestine): Ve-VIIIe siècle; typologie architecturale et aménagements liturgiques;(avec catalogue des monuments).* Turnhout: Brepols; 2001.
- March C. *Spatial and religious transformations in the late antique polis: a multi-disciplinary analysis with a case-study of the city of Gerasa.* Oxford: Archaeopress; 2009.
- Talgam R. *Mosaics of faith: floors of pagans, jews, Samaritans, Christians and Muslims in the Holy Land.* Philadelphia: Pennsylvania State University Press; 2014.
- Haensch R, Lichtenberger A, Raja R. *Christen, Juden und Soldaten im Gerasa des 6. Jahrhunderts Chiron.* 2016;46:177–204.
- Lichtenberger A, Raja R. From synagogue to church: the appropriation of the synagogue of Gerasa/Jerash under Justinian. *Jahrb Antike Christentum.* 2018;61:85–98.
- Joyce H. A mosaic from Gerasa in Orange, Texas, and Berlin. Darmstadt: Verlag Philipp von Zabern; 1980.
- Kriseleit. *Antike Mosaiken: Altes museum, Pergamonmuseum, Antikensammlung Staatliche Museen zu Berlin.* Darmstadt: Philipp von Zabern; 2000.

23. Grossmann RA. A New Reconstruction of a Mosaic from Gerasa. *Yale Univ Art Gall Bull.* 2006; 148–153.
24. Dunbabin KMD. *Mosaics of the Greek and Roman World.* Cambridge: Cambridge University Press; 1999.
25. Moropoulou A, Bakolas A, Bisbikou K. Characterization of ancient, byzantine and later historic mortars by thermal and X-ray diffraction techniques. *Thermochim Acta.* 1995;269:779–95.
26. Daugbjerg TS, et al. Radiocarbon dating of lime plaster from a Roman period cistern in ancient Gerasa, Jerash in Jordan. *J Archaeol Sci Rep.* 2022;42:103373.
27. Beruto DT, Vecchiattini R, Giordani M. Solid products and rate-limiting step in the thermal half decomposition of natural dolomite in a CO₂(g) atmosphere. *Thermochim Acta.* 2003;405:183–94.
28. Beruto DT, Vecchiattini R, Giordani M. Effect of mixtures of H₂O (g) and CO₂ (g) on the thermal half decomposition of dolomite natural stone in high CO₂ pressure regime. *Thermochim Acta.* 2003;404:25–33.
29. Arce, I. Late antique and Umayyad quarries in the Near East. A model of optimization of resources. in *Arqueología de la construcción IV: las canteras en el mundo antiguo: sistemas de explotación y procesos productivos: Actas del congreso de Pavoda, 22–24 de noviembre de 2012 383–412* (Instituto de Arqueología de Mérida, 2014).
30. El-Turki A, Ball RJ, Wang CF, Allen G. Effects of additives in lime-based mortar and paste. *J Build Limes Forum.* 2008;15:48–56.
31. Raw-Rees S, Pesce GLA, Ball RJ, Fodde E. Characterization of binders in the historic lime mortars and plasters from 1A Royal Crescent, Bath. *J Build Limes Forum.* 2012;19:28–37.
32. Pesce G, et al. Radiocarbon dating of lumps from aerial lime mortars and plasters: methodological issues and results from San Nicolò of Capodimonte Church (Camogli, Genoa, Italy). *Radiocarbon.* 2009;51:867–72.
33. Secco M, et al. Mineralogical clustering of the structural mortars from the Sarno Baths, Pompeii: a tool to interpret construction techniques and relative chronologies. *J Cult Herit.* 2019;40:265–73.
34. Secco M, et al. Technological transfers in the Mediterranean on the verge of Romanization: insights from the waterproofing renders of Nora (Sardinia, Italy). *J Cult Herit.* 2020;44:63–82.
35. Kalaitzoglou G, Lichtenberger A, Raja R. The Danish-German Jerash North-West quarter project 2013: preliminary field report. *Annu Dep Antiq Jordan.* 2014;58:11–37.
36. Lichtenberger A, Raja R. A view of Gerasa/Jerash from its Urban Periphery The Northwest Quarter and its significance for the understanding of the urban development of Gerasa from the Roman to the Early Islamic period. *Archaeol Hist Jerash 100 Yrs Excav Jerash Jerash Pap.* 2018;1:143–66.
37. Lichtenberger A, Raja R. The Danish-German Jarash North-West Quarter project: results from the 2014–2015 Seasons. *Stud Hist Archaeol Jordan.* 2019;13:51–71.
38. Kalaitzoglou G, Lichtenberger A, Möller H, Raja REC. Preliminary Report of the Sixth Season of the Danish-German Jerash Northwest Quarter Project 2016. 2022.
39. Kalaitzoglou G, Lichtenberger A, Möller H, Raja R, Bangsgaard P, Eger C, Merkel S, Prange M, Springer A, Polla SLJM. Preliminary Report of the Fifth Season of the Danish-German Jerash Northwest Quarter Project 2015. 2022.
40. Hamarneh C, Abu-Jaber N. Mosaic pavement mortar production in Gerasa in the Byzantine period. *Archaeol Res Asia.* 2017;9:22–33.
41. Rispoli C, et al. The ancient Pozzolanic mortars of the thermal complex of Baia (Campi Flegrei, Italy). *J Cult Herit.* 2019;40:143–54.
42. Fuertes-Prieto MN, et al. The Escalada formation: characterization of a potential chert supply source in the Cantabrian Mountains (NW Spain) during prehistory. *J Lithic Stud.* 2016;3:309–26.
43. El-Turki A, Ball RJ, Allen GC. The influence of relative humidity on structural and chemical changes during carbonation of hydraulic lime. *Cem Concr Res.* 2007;37:1233–40.
44. El-Turki A, Carter MA, Wilson MA, Ball RJ, Allen GC. A microbalance study of the effects of hydraulicity and sand grain size on carbonation of lime and cement. *Constr Build Mater.* 2009;23:1423–8.
45. Secco M, et al. The evolution of the vitruvian recipes over 500 years of floor-making techniques: the case studies of the Domus delle Bestie Ferite and the Domus di Tito Macro (Aquilaia, Italy). *Archaeometry.* 2018;60:185–206.
46. Stefanidou M, Papayianni I, Pachta V. Evaluation of inclusions in mortars of different historical periods from Greek monuments. *Archaeometry.* 2012;54:737–51.
47. Stefanidou M, Papachristoforou M, Kesikidou F. Fiber-reinforced lime mortars. In *Proceedings of the 4th Historic Mortars Conference (HMC 2016): 10th–12th October 2016, Santorini, Greece.* 2016; 422–430
48. De Luca R, et al. Archaeometric study of mortars from the Garum shop at Pompeii, Campania, Italy. *Geoarchaeology.* 2015;30:330–51.
49. Rispoli C, et al. Unveiling the secrets of Roman craftsmanship: mortars from Piscina Mirabilis (Campi Flegrei, Italy). *Archaeol Anthropol Sci.* 2020;12:1–18.
50. Figueiredo C. Properties and performance of lime mortars for conservation: the role of binder chemistry and curing regime. PhD Thesis, University of Bath. 2018.
51. Margalha MG, et al. Microstructural changes of lime putty during aging. *J Mater Civ Eng.* 2013;25:1524–32.
52. El-Turki A, Ball RJ, Holmes S, Allen WJ, Allen GC. Environmental cycling and laboratory testing to evaluate the significance of moisture control for lime mortars. *Constr Build Mater.* 2010;24:1392–7.
53. Pesce GL, et al. Carbonation of hydrous materials at the molecular level: a time of flight-secondary ion mass spectrometry, Raman and density functional theory study. *Cryst Growth Des.* 2017;17:1036–44.
54. Pesce GLA, Ball RJ, Quarta G, Calcagnile L. Identification, extraction, and preparation of reliable lime samples for 14C dating of plasters and mortars with the “pure lime lumps” technique. *Radiocarbon.* 2012;54:933–42.
55. D’Ambrosio E, Marra F, Cavallo A, Gaeta M, Ventura G. Provenance materials for Vitruvius’ harenae fossiciae and pulvis puteolanis: geochemical signature and historical–archaeological implications. *J Archaeol Sci Rep.* 2015;2:186–203.
56. Jackson M, Marra F. Roman stone masonry: volcanic foundations of the ancient city. *Am J Archaeol.* 2006;110:403–36.
57. Thomsen KD. Mortar and plaster production in Jerash: changing perspective from macro to micro. In: Raja R, Sindbak SM, editors. *Urban network evolutions: towards a high-definition archaeology.* Aarhus: Aarhus Universitetsforlag; 2018. p. 109–15.
58. Vejmelková E, Keppert M, Rovnaníková P, Keršner Z, Černý R. Application of burnt clay shale as pozzolan addition to lime mortar. *Cem Concr Compos.* 2012;34:486–92.
59. Ji J, Ge Y, Balsam W, Damuth JE, Chen J. Rapid identification of dolomite using a Fourier Transform Infrared Spectrophotometer (FTIR): a fast method for identifying Heinrich events in IODP Site U1308. *Mar Geol.* 2009;258:60–8.
60. Cizer Ö, et al. Phase and morphology evolution of calcium carbonate precipitated by carbonation of hydrated lime. *J Mater Sci.* 2012;47:6151–65.
61. Taylor D. Calcium carbonate in cholesterol gallstones: polymorphism, distribution, and hypotheses about pathogenesis*1. *Hepatology.* 1995;22:488–96.
62. Ferraz E, Gamelas JAF, Coroado J, Monteiro C, Rocha F. Recycling waste seashells to produce calcitic lime: characterization and wet slaking reactivity. *Waste Biomass Valor.* 2019;10:2397–414.
63. Ghosh SN. IR spectroscopy. In *handbook of analytical techniques in concrete science and technology.* Amsterdam: Elsevier; 2001. p. 174–204.
64. Vizcayno C, de Gutiérrez RM, Castello R, Rodríguez E, Guerrero CE. Pozzolan obtained by mechanochemical and thermal treatments of kaolin. *Appl Clay Sci.* 2010;49:405–13.
65. Makó É, Frost RL, Kristóf J, Horváth E. The effect of Quartz content on the mechanochemical activation of kaolinite. *J Colloid Interface Sci.* 2001;244:359–64.
66. Wootton WT. The mosaics: in-situ floors and fragments in Jerash. In *architectural elements, wall paintings, and mosaics. Final Publications* (eds. A. Lichtenberger & Raja, R.) (The Danish-German Jerash Northwest Quarter Project IV).
67. Kondoleon C. *Domestic and divine: Roman mosaics in the house of Dionysos.* Ithaca: Cornell University Press; 1994.
68. Dochia M, Roskwitalski Z. *Handbook of natural fibres: types, properties and factors affecting breeding and cultivation.* Sawston: Woodhead Publishing; 2012.
69. Kennedy D. The identity of Roman Gerasa: an archaeological approach. *Mediterr Archaeol.* 1998;11:39–69.

70. Chakraborty S, et al. Improvement of the mechanical properties of jute fibre reinforced cement mortar: a statistical approach. *Constr Build Mater.* 2013;38:776–84.
71. Sfiligoj Smole M, Hribnik S, Stana Kleinschek K, Kreže T. Plant fibres for textile and technical applications. In: Grundas S, editor. *Advances in agrophysical research*. Intech: Rijeka; 2013. p. 369–98.
72. Uscatescu A, Manuel M. The Macellum of Gerasa (Jerash, Jordan): from a market place to an industrial area. *Bull Am Sch Orient Res.* 1997;307:67–88.

Publisher's Note

Springer Nature remains neutral with regard to jurisdictional claims in published maps and institutional affiliations.